

High-Precision Position Control of a Heavy-Lift Manipulator in a Dynamic Environment

by

Justin R. Garretson

Bachelor of Science in Engineering with Honors, Mechanical and Aerospace Engineering  
Princeton University, 2003

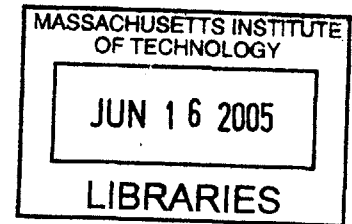
Submitted to the Department of Mechanical Engineering  
in Partial Fulfillment of the Requirements for the Degree of  
Master of Science

at the

Massachusetts Institute of Technology

June 2005

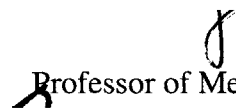
© Massachusetts Institute of Technology  
All Rights Reserved



Signature of Author .....

Department of Mechanical Engineering  
April 8th, 2005

Certified by .....

 Steven Dubowsky  
Professor of Mechanical Engineering  
Thesis Advisor

Accepted by .....

Professor Lallit Anand  
Chairman, Committee on Graduate Studies

**BARKER**

# High-Precision Position Control of a Heavy-Lift Manipulator in a Dynamic Environment

by

Justin R. Garretson

Submitted to the Department of Mechanical Engineering  
on April 1st, 2005, in Partial Fulfillment of the  
Requirements for the Degree of  
Master of Science

## ABSTRACT

This thesis considers the control of a heavy-lift serial manipulator operating on the deck of a large ocean vessel. This application presents a unique challenge for high-precision control because the system must contend with both high levels of joint friction and oscillatory motions in the manipulator's base. Due to the uncontrolled outdoor environment, the behavior of these disturbances in the field cannot be accurately predicted using models developed offline. To achieve high-precision control, the system must therefore be capable of effectively estimating and compensating for these disturbances online.

This thesis presents the design of a position control system to allow high-precision control of the manipulator's payload by a human user. The design features a standard decentralized linear control architecture augmented by a combination of adaptive and sensor-based techniques to estimate and compensate for base-motions and joint friction. A procedure is also suggested by which a parametric friction model can be extracted from adaptive estimates recorded over a period of time. This extracted model can be used to temporarily replace the adaptive estimation in compensating for joint friction when the manipulator is in contact with the environment.

Performance of the control methods developed here are evaluated using simulation studies conducted with a high-fidelity dynamic model of the mechanical system. These studies demonstrate the tracking capability of the control system for various representative tasks.

Thesis Supervisor: Steven Dubowsky, Professor of Mechanical Engineering

## **ACKNOWLEDGEMENTS**

I would like to thank Foster Miller Inc. for their support in the design of this system. I would like to thank my collaborators on this project including Matthew Dicicco, William Becker, and Mikael Fridenfalk. Special thanks go out to Dr. Karl Iagnemma and Dr. Matthew Lichter for their mentorship and technical assistance during this project, and all the other members of the Field and Space Robotics Laboratory for their technical guidance and friendship. Of course, the biggest thanks are due to the esteemed Dr. D for his guidance and for giving me the opportunity to work on this project.

I would like to dedicate this thesis to my mother and father who have given me so much love and opportunity. Thanks for making everything possible.

# CONTENTS

---

ABSTRACT.....	2
ACKNOWLEDGEMENTS .....	3
CONTENTS .....	4
FIGURES .....	7
TABLES .....	9
CHAPTER 1: INTRODUCTION .....	10
1.1 Introduction.....	10
1.2 Application-Specific Control Challenges .....	10
1.2.1 Joint Friction.....	11
1.2.2 Base Motions .....	11
1.2.3 Other Environmental Factors.....	12
1.2.4 Contact Forces .....	12
1.3 Background and Literature Review .....	13
1.3.1 Friction Compensation.....	14
1.3.2 Base-motion Compensation.....	15
1.4 Goals of this Thesis .....	16
1.5 Thesis Outline.....	17
CHAPTER 2: POSITION CONTROL METHODS.....	18
2.1 Introduction.....	18
2.2 Mechanical System Description and Assumptions.....	19
2.3 Cartesian Control.....	22

2.3.1 Resolved-Rate Control.....	22
2.3.2 Manipulator Kinematics .....	23
2.3.3 Workspace Singularities .....	26
2.4 Joint Control .....	27
2.4.1 PID Control.....	27
2.4.2 Gain Scheduling.....	30
2.4.3 Joint Modeling and Gain Tuning.....	30
2.4.4 Structural Resonance and Controller Bandwidth .....	33
<b>CHAPTER 3: COMPENSATING FOR DISTURBANCES .....</b>	<b>35</b>
3.1 Introduction.....	35
3.2 Compensating for Gravity .....	35
3.3 Compensating for Ship Motions.....	37
3.4 Modeling Joint Friction .....	39
3.4.1 Static-Load-Dependent Model (Joints 1-3) .....	39
3.4.2 Torque-Dependent Model (Joints 4-6) .....	42
3.5 Sensor-based Friction Compensation (Joints 1-3).....	43
3.5.1 Friction Estimation Using Load Cells .....	43
3.5.2 Torque Control.....	45
3.6 Adaptive Friction Compensation (Joints 4-6).....	48
3.7 Contact Forces and Friction Model Extraction.....	52
<b>CHAPTER 4: SIMULATION RESULTS .....</b>	<b>54</b>
4.1 Introduction.....	54
4.2 Simulation Setup.....	54
4.3 Simulation Results .....	56

4.3.1 Representative Heavy-Payload Task .....	56
4.3.2 Representative Light-Payload Task.....	61
4.3.3 Resolution Study.....	65
4.3.4 Repeatability Study.....	67
4.3.5 Preliminary Analysis of Ship Motion Effects.....	69
4.3.6 Friction Model Extraction.....	72
4.4 Summary and Conclusions .....	76
<b>CHAPTER 5: CONCLUSIONS AND FUTURE WORK.....</b>	<b>78</b>
5.1 Contributions of this Work.....	78
5.2 Suggestions for Future Work.....	79
<b>REFERENCES .....</b>	<b>81</b>
<b>APPENDIX A: MANIPULATOR PARAMETERS .....</b>	<b>84</b>
<b>APPENDIX B: CONTROLLER PARAMETERS .....</b>	<b>86</b>
<b>APPENDIX C: SIMULATED FRICTION PARAMETERS .....</b>	<b>88</b>

## **FIGURES**

---

- 2.1. Manipulator joint definitions (courtesy of Foster Miller Inc.)
- 2.2. Definition of manipulator reference frames (adapted from Foster Miller Inc.)
- 2.3. Resolved-rate control architecture
- 2.4. Joint control architecture
- 2.5. Joint model used in designing the PID joint controllers
- 2.6. Joint control architecture with transfer functions defined
- 2.7. Reduced closed-loop transfer function for joint control
- 3.1. Joint control with feed-forward gravity compensation
- 3.2. Joint control with feed-forward gravity and ship motion compensation
- 3.3. Stribeck effect in the static-load-dependent friction model
- 3.4. Location of load cells in joints 1-3 (adapted from Foster Miller Inc.)
- 3.5. Torque control architecture (joints 1-3)
- 3.6. Simplified representation of the torque control architecture
- 3.7. Root-locus for the PI torque controllers
- 3.8. Joint model for the formulation of the Friedland-Park estimation method
- 3.9. Joint control architecture with adaptive friction estimation and compensation
- 3.10. Joint control with feed-forward friction compensation using models extracted from estimator data
- 4.1. Structure of the position control simulation process
- 4.2. End-effector trajectory in base-coordinates for the representative heavy-payload task
- 4.3. Translational end-effector tracking error during the representative heavy-payload task
- 4.4. Position of joint 5 during the representative heavy-payload task

- 4.5. Comparison of tracking error with and without friction compensation
- 4.6. End-effector trajectory in base-coordinates for the representative light-payload task
- 4.7. Translational end-effector tracking error during the representative light-payload task.
- 4.8. Position of joints 1, 5, and 6 during the representative light-payload task
- 4.9. End-effector tracking a 1cm square wave with and without friction compensation
- 4.10. End-effector trajectory, tracking 25 random motions from a set-point
- 4.11. End-effector positions after each random motion and 2 seconds of settling time, with and without friction compensation
- 4.12. Application of base rotations to the simulated manipulator model (adapted from Foster Miller Inc.)
- 4.13. Translational tracking error with simulated base motions
- 4.14. Identification of friction parameters using recorded friction estimates: magnitude of simulated friction
- 4.15. Identification of friction parameters using recorded friction estimates: magnitude of simulated friction w/ friction estimates
- 4.16. Identification of friction parameters using recorded friction estimates: magnitude of simulated friction w/ filtered friction estimates
- 4.17. Identification of friction parameters using recorded friction estimates: magnitude of simulated friction w/ filtered friction estimates and curve-fit
- 4.18. Identification of friction parameters using recorded friction estimates: magnitude of simulated friction w/ filtered friction estimates, curve-fit, and predicted friction profile
- A.1. Definition of joint coordinate systems with all joint angles at zero (courtesy of Foster Miller Inc.)

## TABLES

---

- 4.1. Target performance specifications for the representative heavy-payload task
- 4.2. Tracking error results for the representative heavy-payload task
- 4.3. Target performance specifications for the representative light-payload task
- 4.4. Tracking error results for the representative light-payload task
- 4.5. Translational error results for the repeatability study
- 4.6. Periods and amplitudes for simulated base rotations
- 4.7. Periods and amplitudes for simulated translational base accelerations
- 4.8. Error results for the extracted friction model
- A.1. Denavit-Hartenberg manipulator parameters (courtesy of Foster Miller Inc.)
- A.2. Inertial link parameters (courtesy of Foster Miller Inc.)
- A.3. Inertial payload parameters (courtesy of Foster Miller Inc.)
- B.1. PID gains for the representative heavy-payload task
- B.2. PID gains for the representative light-payload task
- B.3. Integral saturation limits
- B.4. PI torque-control gains
- B.5. Friedland-Park estimator gains
- C.1. Parameters for simulated static-load-dependent friction
- C.2. Parameters for simulated torque-dependent friction

# CHAPTER 1

## INTRODUCTION

---

### 1.1 Introduction

This thesis presents the design of a position control system for a heavy-lift serial manipulator being developed commercially. This manipulator is intended for use on the deck of large sea vessels in widely varying weather conditions. The control system will allow a human user to control the velocity and direction of the manipulator's payload in the field. The design employs a combination of sensor-based and adaptive techniques for estimation and compensation of the large dynamic disturbances associated with this manipulator and its operational environment. Significant disturbances include (but are not limited to) ship motions and friction in the manipulator's joints, both of which will be time-variant and difficult to predict due to environmental factors. This controller design includes a robust and effective means of estimating and compensating for these disturbances online, thereby making precise and repeatable positioning of the manipulator's payload possible.

### 1.2 Application-Specific Control Challenges

High-precision manipulation is a very well studied problem in general. The particular manipulation task considered in this thesis, however, contains several aspects that create unique challenges for control. These challenges primarily take the form of dynamic disturbances imparted on the manipulator due to factors relating to both the external environment and the manipulator itself. These disturbances must somehow be compensated to successfully meet the precision requirements for this manipulator system.

## **1.2.1 Joint Friction**

Joint friction presents one of the most difficult challenges for high-precision control [Olsson, et al, 1998]. The manipulator in this project is a heavy-lift manipulator expected to lift and move payloads weighing up to 3000 lbs. To generate the large joint torques necessary to move under such heavy loads, the manipulator uses very highly geared electric motors. A large amount of friction is produced in the bearings of each joint, the heavy transmissions, and the electric motors themselves. These friction torques also have complex profiles including (at the very least) dependencies on manipulator position, velocity, payload mass, and motor torque. In addition, the parameters of the joint friction can change over time due to unpredictable effects like temperature change, wear in the mechanical components, rain, sea salt, etc. The end result is a manipulator with large levels of joint friction that are extremely difficult to accurately model and predict.

Joint friction is an important concern for position control because it makes it difficult for the manipulator to make smooth and precise motions. In order to meet the performance requirements for this manipulator, it is critical that the position controller have the ability to effectively compensate for these effects. Finding a robust and effective method to estimate and compensate for friction in the manipulator's joints is a critical challenge in the design of this control system.

## **1.2.2 Base Motions**

Another critical control issue in this design is that the base of the manipulator does not remain stationary in inertial space while the payload is being moved. The manipulator is designed for operation on the deck of a ship, and while the manipulator's base does remain fixed with respect to the ship's deck, the ship itself is subject to continuous and potentially large dynamic motions due to wind and sea conditions. These motions will impart accelerations on the manipulator and its payload which will be seen as disturbances by the position controller. The position controller will need to effectively compensate for these motions for the manipulator to perform its task successfully.

### **1.2.3 Other Environmental Factors**

Because of the manipulator's uncontrolled outdoor environment, there is a high potential for random disturbances that are difficult or impossible to model. Wind, in particular, is almost always present to some degree and exerts a disturbance on the manipulator and its payload. Other random disturbances can include objects or even people inadvertently falling or leaning against the manipulator.

Perhaps the most important challenge associated with this manipulator's environment is the effect that it can have on joint friction. Rain, salt from the ocean, and changes in ambient temperature can all have significant effects on the behavior of friction experienced in the manipulator's joints. These effects make it virtually impossible to accurately estimate joint friction in the field using open-loop methods.

### **1.2.4 Contact Forces**

Another important consideration in the design of this controller is the effect of contact forces between the payload and the environment. Contact forces necessarily occur each time the manipulator picks up a payload or places a payload back into the environment. Most objects in the manipulator's environment are assumed to be rigid and therefore it is impossible to compensate for these forces in the same way that forces like friction are compensated. An attempt by the control system to do so could in fact result in damage to the manipulator and/or the environment.

This is an important consideration when employing closed-loop methods of disturbance compensation. To eliminate the possibility of instability and/or damage, the effects of contact forces must be kept outside of any disturbance-feedback loops used in the controller. If this cannot be done, then these feedback loops must be deactivated and/or replaced by open-loop compensation in the presence of contact forces.

## 1.3 Background and Literature Review

The particular manipulator application considered in this thesis has been studied extensively in recent years at the Oak Ridge National Laboratory [Deeter, et al, 1997, Love, et al, 2003/2004]. The work at ORNL has included the development of control algorithms for ORNL's Next Generation Munitions Handler, a prototype heavy-lift manipulator platform developed at ORNL for use on naval vessels. Research at ORNL has explored the use of various position and force control strategies for human amplification with the NGMH platform with favorable results.

The various control challenges considered in this thesis have also been studied individually over the past thirty years. High-precision Cartesian control has been achieved on a multitude of manipulator platforms using a broad range of control approaches. The most common industrial control solution to date remains the PID (proportional-integral-derivative) architecture, enhanced with performance-increasing features like integral saturation and partial feed-forward dynamic compensation [Visioli, 2002]. The familiarity of PID control, coupled with the extensive framework available for its analysis and implementation, has allowed it to remain the preferred solution for industrial applications despite the emergence of more innovative solutions.

More advanced global tracking solutions include methods like sliding mode control, neural-network-based control, and model-based methods like state-feedback and computed torque control [Khosla, 1988, Huang, et al, 2002, Visioli, 2002]. In addition, a variety of model-based adaptive schemes have been developed to allow the application of model-based methods in systems with unknown dynamics [Landau, 1974, Astrom, 1983, Slotine, 1987]. Each of the proposed methods has unique strengths and varies in effectiveness depending on the nature of the mechanical system and its application.

Model-based controllers can potentially provide performance far superior to what is achievable with decentralized linear control, but they also require considerably more complexity. In addition, there are problems with analysis and implementation of many of these nonlinear methods that have not yet been fully solved. In considering the use of model-based control for a given application, it is necessary to ask whether the potential

benefit in performance is worth the additional complexity and problems with implementation.

### **1.3.1 Friction Compensation**

Joint friction is often a limiting factor in high-performance manipulator control. To improve manipulator performance, many control methods have been suggested to help systems estimate and compensate for the effects of joint friction [Armstrong, et al, 1994]. The majority of these methods fall into three categories: model-based compensation, sensor-based compensation, and torque bias/pulse injection.

Model-based friction compensation uses mathematical models to predict the effects of friction online. Using the predicted values of the friction force/torque, the effects of friction can then be compensated with motor torques [Gomes, et al, 2003, Moreno, et al, 2003]. The effectiveness of this type of compensation method depends directly on the accuracy of the predictor models. To improve the accuracy of these models, extensive work has been done to advance the understanding of joint friction behavior and to develop mathematical models offline that accurately represent this behavior [Olsson, et al, 1998]. Despite these efforts, the effectiveness of these offline models in predicting joint friction in the field is fundamentally limited by their inability to track changes in the friction model over time. Environmental factors and changes in the mechanical system over time can cause the joint friction behavior to deviate from what was observed during offline modeling. To compensate for these online variations, numerous methods have been proposed for online estimation of friction parameters including both adaptive-based and observer-based approaches [Armstrong, et al, 1994, Canudas, et al, 1997, Henrichfreise, et al, 1998, Friedland, et al, 1993]. These methods take advantage of known or measured information about the system dynamics to identify friction parameters online. Online parameter identification has been demonstrated to allow very high performance in systems with high joint friction [Canudas, et al, 1987, Lischinsky, et al, 1997, Kim, et al, 2002]. The formulation of most adaptive methods is very complex,

however, especially for high-degree-of-freedom systems [Niemeyer, et al, 1988]. For this reason, adaptive identification is not practical for some systems.

Sensor-based compensation is generally considered a luxury in control systems. These methods can be employed when there are sensors available to provide direct feedback of the friction experienced in the system. Torque control is the most common form of sensor-based compensation [Luh, et al, 1983, Pfeffer, et al, 1989]. This method involves the formation of torque control loops around a manipulator's joints. Sensors measure the torque applied to the joint and feed this back to the torque controllers which adjust the motor signal accordingly. No model of the friction is required and yet the compensation is robust to changes in the friction over time. This method has been shown to provide extremely accurate compensation for joint friction and is the preferred approach whenever the system hardware allows. More recently, an alternative sensor-based method has been proposed that allows the friction in all joints to be identified using a single 6-DOF force/torque sensor in the manipulator's base [Iagnemma, 1997], thus greatly simplifying the hardware implementation of sensor-based approaches. This method, called Base-Sensor Control, has been shown in experiments to provide identification of joint friction in a Puma robot approaching the resolution of the joint encoders [Morel, et al, 2000, Meggiolaro, et al, 2001].

The third major category of friction compensation involves the introduction of a pulse or high-frequency bias to the applied joint torque sufficient to cause small joint displacements [Armstrong, et al, 1994]. This helps to overcome static friction and also has been shown to smooth the friction profile at low velocities. Although not as effective as model or sensor-based compensation, this can provide significant performance benefits with far less added effort and complexity than the previously described methods.

### **1.3.2 Base-motion Compensation**

Most of the work on base-motion compensation in the literature is concerned with incorporating base motions into the calculation of the manipulator kinematics and/or the desired payload trajectory [Dubowsky, et al, 1987, Tahboub, 1997, Agostini, et al, 2002].

This is because the major concern is usually that the manipulator coordinate system is moving relative to the workspace. For this application the problem is different because it is assumed that the workspace and the manipulator base-coordinates both move together. The concern is therefore not the payload trajectory but rather the dynamic effects of the large oscillatory rotations and G-loads experienced by the manipulator due to the motion of the ship.

Relatively little work has been done previously in modeling and/or compensating for the dynamic effects of oscillatory ship motions in manipulator control [Love, et al, 2003/2004, Toda, 2004]. Some of the largest contributions in this area have come from the ongoing research at the Oak Ridge National Laboratory. This work has produced new methods of modeling and compensating for ship motions that use repetitive and adaptive learning techniques to identify the ship motions without the use of sensors. Preliminary simulations of these methods on a three-degree-of-freedom manipulator have yielded favorable results [Love, et al, 2003/2004] and are an ongoing effort at ORNL.

The work in this thesis does not attempt to advance existing methods of base-motion compensation or propose new ones. For this project, basic sinusoidal models of the expected ship motions were provided by the developers of the mechanical system and used for analysis. The compensation method used here involves measuring the base-motions with sensors and calculating feed-forward compensation torques for each joint using a quasi-static model of the manipulator [Sciavicco, et al, 2000]. This compensation technique has been employed in the work at ORNL where it was shown to provide significant improvements in controller performance during simulation [Love, et al, 2003].

## **1.4 Goals of this Thesis**

The goal of this thesis is to present a design solution for achieving robust and repeatable high-precision position control with a heavy-lift manipulator operating on the deck of a large sea vessel in varying weather conditions. This thesis places an emphasis on the use of combined sensor-based and adaptive methods for identifying and compensating for joint friction and other dynamic disturbances associated with this

manipulator and its unique work environment. Finally, it is the goal of this thesis to validate the potential of this controller design with the results of high-fidelity dynamic simulations.

## **1.5 Thesis Outline**

The complete architecture of the position control system presented in this thesis is covered in the two chapters following this introduction. Chapter 2 describes the basic mechanical system and how movement commands from a human operator are translated by the control system into the joint torques necessary to produce the desired motions. Chapter 3 covers all methods associated with the modeling, estimation, and compensation of the major dynamic disturbances affecting the manipulator.

Chapter 4 contains the results of various simulations that were used to test the position control system using a high-fidelity dynamic model of the manipulator system. These simulations include studies of the control system's tracking capability with special attention to repeatability, resolution, and effectiveness in compensating for joint friction and ship motions.

The final Chapter discusses the contributions of this thesis and plans for future work with the control system. Several appendices are also provided. Appendix A contains a listing of the complete kinematic and inertial parameters of the manipulator. Appendix B contains a listing of the control system parameters used in simulation. Appendix C provides the parameter values used in the simulation of joint friction for this project.

# CHAPTER 2

## POSITION CONTROL METHODS

---

### 2.1 Introduction

In the context of robotic manipulators, “position control” refers to the act of commanding a manipulator’s actuated links in order to follow prescribed trajectories. Multiple links within a manipulator can be controlled independently or together to create coordinated motions. The exact nature of a position controller will depend on both the nature of the manipulator itself and the intended application.

The purpose of this chapter is to describe the fundamental control methods used to achieve position control for this manipulator and to briefly cover the important principles involved in these methods. Algorithms specifically involved in compensating for disturbances will not be included in this discussion. The estimation and compensation of dynamic disturbances is treated as a special topic and is covered in detail in Chapter 3.

The first part of this chapter contains a basic description of the mechanical system. This description is accompanied by a statement of the key assumptions that have been made about the mechanical system for the purposes of this controller design. The second part of this chapter describes the form of the human user’s command inputs and how these inputs are interpreted by the position control system to compute the necessary joint torques. The final section of this chapter describes the design of the feedback loops used to control the individual manipulator joints.

## 2.2 Mechanical System Description and Assumptions

The mechanical system to be controlled consists of a six-link serial manipulator mounted on a mobile platform. The six links are connected in series via five rotational joints and one translational (prismatic) joint as shown in Figure 2.1. The complete kinematic and inertial parameters of the mechanical system are provided in Appendix A.

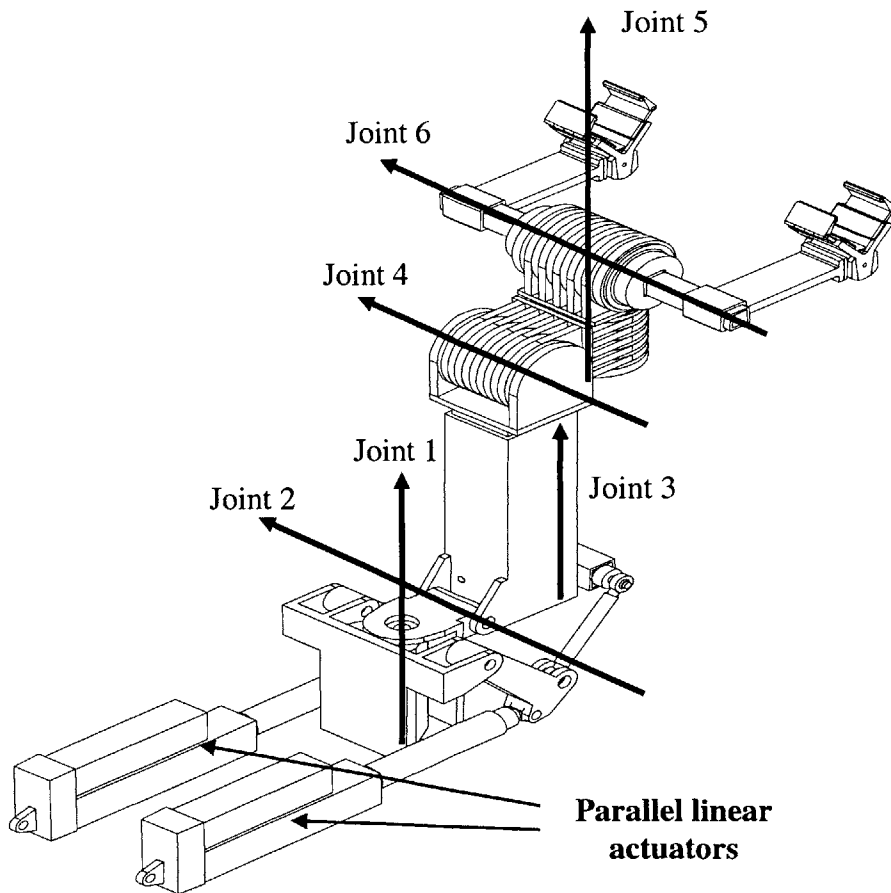


*Figure 2.1. Manipulator joint definitions  
(courtesy of Foster Miller Inc.)*

Joints 1 and 2 control the yaw and pitch of the entire manipulator, respectively. These two joints are controlled simultaneously by two parallel linear actuators at the base of the manipulator as seen in Figure 2.1. Joint 3 is a translational joint that allows the manipulator to extend or retract in a linear manner. At the end of this joint are three more rotational joints allowing additional pitch, yaw, and roll motions of the payload. Using

all six joints, the manipulator can move a payload through all 6 degrees of freedom in 3D space.

Joints 4, 5, and 6 are direct-drive, meaning that the motions of the joint and the motor actuating the joint are the same. Joints 1, 2, and 3, however, are highly geared. For each of these three joints, an electric motor acts through an intermediate transmission to turn a roller-screw. In joint 3, the roller-screw controls the motions of the translational joint directly. In joints 1 and 2, however, two roller-screws act through the linkage mechanism shown in Figure 2.1 to actuate these two joints simultaneously.

Payloads are secured at the end of the manipulator in different ways depending on the nature of the payload. Lighter payloads can be secured using the two grippers shown at the ends of the fork-tines attached to joint 6 in Figure 2.1. For heavier payloads, these grippers can be removed and the payload can be lifted on top of a pallet using the fork-tines themselves. Payloads for this manipulator range in mass from 0 – 3000 lbs.

The relevant sensing capability of the mechanical system includes the following:

1. One encoder at each joint (six total) to measure the joint positions.
2. Two inclinometers in the manipulator's base to measure pitch and roll due to ship motions.
3. One 3D translational accelerometer in the manipulator's base to measure acceleration of the manipulator due to ship motions.
4. One load cell installed in each of the manipulator's three roller-screw transmissions (joints 1-3). Cells are inserted at the end of the roller-screws nearest the joint and measure the axial force at the cell's location.

In designing the position control system for this manipulator, the following assumptions about the physical system are made:

1. Payload motions are commanded manually by a human operator through a joystick.
2. All payload motions are achieved through the individual or combined motion of the six actuated joints defined in Figure 2.1.

3. The mobile platform supporting the manipulator remains fixed relative to its environment during all manipulator motions (though the environment may be moving relative to the world).
4. All joints in the manipulator are back-drivable.

The reference frame for the manipulator is the “base” coordinate system defined in Figure 2.2. An important reference point for the manipulator, called the “end-effector,” is also shown in this figure. This virtual reference point is located at the end of the manipulator’s kinematic chain (end of link 6) and represents the controlled point for the position control system in Cartesian space. The manipulator’s payload is assumed to be fixed at the end-effector.

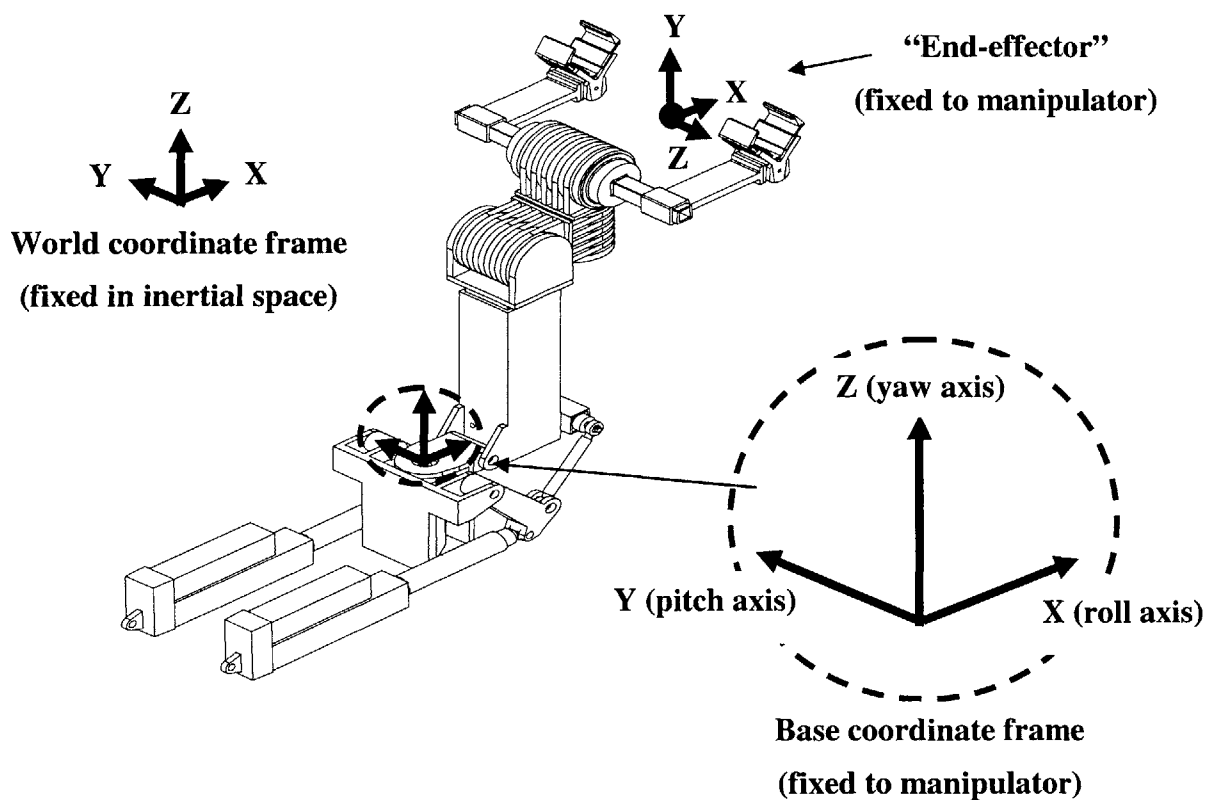


Figure 2.2. Definition of manipulator reference frames (adapted from Foster Miller Inc.)

## 2.3 Cartesian Control

During manipulator operation, the human operator uses joystick inputs to command the payload's movement in space. The operator has the option of commanding the joints individually or commanding the motion of the payload directly. In the latter case, the commanded motion is for the payload only and contains no information about the individual joint motions necessary to produce the desired motion for the payload. It is therefore, the responsibility of the position control system to determine the joint motions required to achieve the desired payload motion.

The domain of 3D space in which the payload motions are commanded is referred to as *Cartesian space*. Similarly, the domain of possible joint movements for all of the manipulator's joints is referred to as *joint space*. Commanding the payload's motion directly is called *Cartesian control* [Sciavicco, et al, 2000] because the input to the controller is given in Cartesian space as opposed to in joint space.

### 2.3.1 Resolved-Rate Control

In this design, a special form of Cartesian control is used called *resolved-rate control* [Whitney, 1969]. In resolved-rate control, the input to the controller is a directed velocity in Cartesian space (refer to Figure 2.3). This is the velocity in Cartesian space that the human user wants the payload to follow. The resolved-rate controller uses its knowledge of the manipulator's geometry to compute the joint velocities necessary to produce the desired Cartesian velocity for the end-effector. The measured quantity at the joints, however, is position rather than velocity, so the controller integrates the desired joint velocities to find the desired joint positions. The controller now has both the desired and the measured positions for each manipulator joint and can employ any number of joint control methods to control the position of each individual joint. Figure 2.3 shows the architecture of the resolved-rate algorithm.

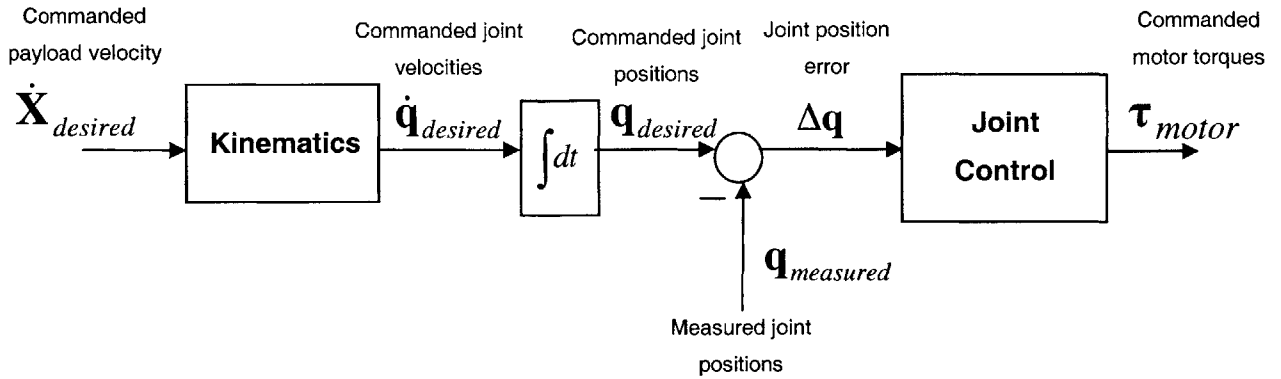


Figure 2.3. Resolved-rate control architecture

The transformation from Cartesian velocity to joint velocity is computed using the manipulator *kinematics*. The following section will discuss in greater detail the role of the manipulator kinematics and how these equations are solved.

### 2.3.2 Manipulator Kinematics

This section is presented as a brief tutorial on manipulator kinematics. The principles described here are well documented in the literature and can be found in most current textbooks on robotic manipulation and control [Paul, 1981, Sciavicco, et al, 2000]. This thesis does not make or claim to make any contributions in this area.

The motion of the manipulator can be described by variables in joint space, Cartesian space, or both. In joint space, the describing variables are the angular positions, velocities, and accelerations of the manipulator’s 6 joints. In Cartesian space, the describing variables are the position, velocity, and acceleration of the manipulator’s end-effector. As mentioned in the previous section, solving the manipulator kinematics allows transformation of these variables back and forth between Cartesian space and joint space. The transformation between these two domains is purely a function of the manipulator’s geometry.

The manipulator kinematic transformations can be separated into two parts: the *forward kinematics* and the *inverse kinematics* [Sciavicco, et al, 2000]. The difference between the forward and inverse kinematics is the direction of transformation. The forward kinematics is used to transform from joint space to Cartesian space. In other words, for a given set of joint angles, the forward kinematic equations are solved to find the corresponding Cartesian position and orientation of manipulator's endpoint. This relationship is described by Equations 2.1 – 2.3 below.

$$\mathbf{X} = F(\mathbf{q}) \quad (2.1)$$

$$\mathbf{X} = \begin{bmatrix} x \\ y \\ z \\ \theta_x \\ \theta_y \\ \theta_z \end{bmatrix} \quad (2.2)$$

$$\mathbf{q} = (q_1, q_2, q_3, q_4, q_5, q_6)^T \quad (2.3)$$

where  $\mathbf{q}$  is the 6x1 vector of joint angles and  $\mathbf{X}$  is the 6x1 vector defining the position and orientation of the manipulator's endpoint in 3D space.

To compute the forward transformation of the velocities in the two domains, the partial derivatives of the function  $F(\mathbf{q})$  are taken with respect to each joint  $q_i$ . The resulting relationship can be written as follows:

$$\frac{d\mathbf{X}}{dt} = \mathbf{J} \frac{d\mathbf{q}}{dt} \quad (2.4)$$

$$\mathbf{J} = \begin{bmatrix} \frac{\partial x}{\partial q_1} & \cdot & \cdot & \cdot & \cdot & \frac{\partial x}{\partial q_6} \\ \cdot & \cdot & & & & \cdot \\ \cdot & & \cdot & & & \cdot \\ \cdot & & & \cdot & & \cdot \\ \cdot & & & & \cdot & \cdot \\ \frac{\partial \theta_z}{\partial q_1} & \cdot & \cdot & \cdot & \cdot & \frac{\partial \theta_z}{\partial q_6} \end{bmatrix} \quad (2.5)$$

The matrix  $\mathbf{J}$  is called the *Jacobian* matrix [Sciavicco, et al, 2000]. This matrix is a function of the joint angles and therefore must be recalculated continuously as the manipulator moves.

For serial manipulators, the forward kinematic transformation (Eq. 2.1) can always be written in closed form. Solving the inverse kinematics, however, presents a more difficult problem. The inverse kinematics is the forward kinematics performed in reverse, allowing calculation of the joint angles based on the position and orientation of the manipulator's end-effector. Multiple methods have been proposed to accomplish this [Buss, 2004]. In this thesis, the inverse kinematic transformation is computed by the *inverse Jacobian* method [Cheah, 2004]. The idea is that if the Jacobian matrix used in the forward kinematics is square (as it is for this manipulator), then it can be inverted to provide the inverse kinematic transformation for the velocities. The resulting relationship is shown in Equation 2.6.

$$\frac{d\mathbf{q}}{dt} = \mathbf{J}^{-1} \frac{d\mathbf{X}}{dt} \quad (2.6)$$

This method is the most direct and provides an exact solution for the joint velocities. The joint positions can then be approximated through integration of the computed velocities. An important drawback of this method, however, is that the Jacobian matrix must be invertible for a solution to be found. In certain manipulator positions, the

Jacobian matrix can become singular and thus cannot be inverted. Such manipulator positions are called *workspace singularities* and are the topic of the next section.

### **2.3.3 Workspace Singularities**

Depending on a manipulator's design, there may be certain poses in which the manipulator's endpoint cannot move and/or rotate in a particular direction no matter how the manipulator's joints move. When this happens, the Jacobian matrix involved in calculating the manipulator's kinematics becomes singular and the inverse Jacobian method cannot be applied [Cheah, 2004]. Manipulator poses that cause the Jacobian matrix to become singular are called workspace singularities. Singularities generally occur when multiple joint axes become parallel and/or the manipulator reaches the fundamental limit of its physical reach (e.g. a fully-extended double-pendulum).

The intended operation of this manipulator is such that only a relatively small region of its workspace is used. This means that most of the workspace singularities for this manipulator will never be encountered and can therefore be ignored. In fact, there is only one singular configuration that affects this manipulator's operation in practice. This singularity occurs whenever joint 5 is rotated such that the axes of joints 4 and 6 become parallel (refer to Figure 2.1). In this configuration, the manipulator loses one rotational degree of freedom because it cannot "roll" the endpoint.

Because the position controller cannot compute the inverse kinematics at a singularity, Cartesian control cannot be used in this location. Instead, the human operator must command the individual joint velocities directly, bypassing calculation of the inverse kinematics altogether. Although it is more difficult for the user to produce complex payload motions in this manner, it will allow him/her to move the manipulator through the singular configuration to a pose where Cartesian control can again be used.

## 2.4 Joint Control

The discussion thus far has been concerned with calculating the joint trajectories necessary to produce the manipulator motions commanded by the human operator. Once the desired joint trajectories are known, the challenge then is to make the joints follow these trajectories with sufficient stability and precision. This task is the responsibility of the joint controllers.

For each of the manipulator's six joints there is an independent controller responsible for the motion of that joint. Each of these joint controllers consists of a feedback loop algorithm using a PID control law. The feedback signal is the angle of the joint measured by the encoder sensor. This measured value is subtracted from the desired value to compute the joint position error. Based on this computed error, the PID control law calculates a motor torque to drive the joint toward its desired position. A diagram of the joint control loop is shown in Figure 2.4.

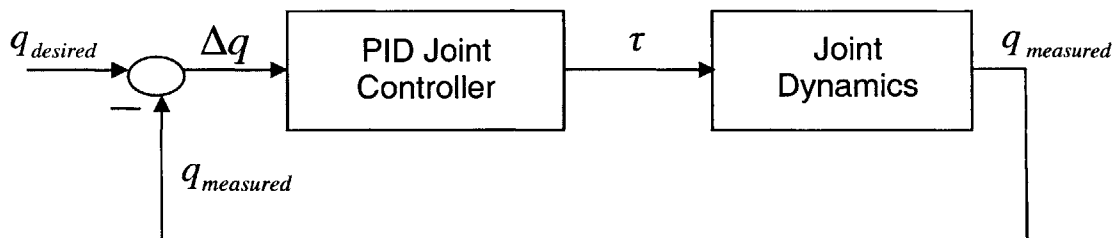


Figure 2.4. Joint control architecture

### 2.4.1 PID Control

All six joint controllers use a PID (proportional-integral-derivative) control law to calculate the control torques from the error in joint position [Astrom, et al, 1995]. In its most basic form, the PID algorithm computes the control torque as a linear function of the position error, the time rate of change of the position error, and the integral of the position error with respect to time. This is represented in the Laplace domain by the following equation:

$$\tau_{PID} = (K_P + K_D s + \frac{K_I}{s})(q_{desired} - q_{measured}) \quad (2.7)$$

where  $K_P$ ,  $K_D$ , and  $K_I$  are constant gains.

The joint controllers in this design use a modified version of the basic PID algorithm shown above. The first important modification involves the derivative term. Rather than multiply the joint error's rate of change by a single gain as in Equation 2.7, the error rate is instead separated into its two components (measured joint velocity and desired joint velocity) and each component is multiplied by a separate gain. The form of the PID algorithm therefore becomes the following:

$$\tau_{PID} = (K_P + \frac{K_I}{s})(q_{desired} - q_{measured}) + K_{D1} s q_{desired} - K_{D2} s q_{measured} \quad (2.8)$$

Or equivalently:

$$\tau_{PID} = (K_P + K_{D1} s + \frac{K_I}{s})(q_{desired} - q_{measured}) + (K_{D1} - K_{D2}) s q_{measured} \quad (2.9)$$

The term  $(K_{D1} - K_{D2}) s q_{measured}$  behaves exactly like viscous damping and thus can be used to add damping to the closed-loop system response. Increasing the gain in this term increases the stability margins of the control system. The term  $K_{D1} s (q_{desired} - q_{measured})$  simulates the effect of a dashpot connecting the joint to its desired position. Increasing the gain in this term both quickens the rise time and reduces overshoot in the closed-loop response to a step input, but also reduces the stability margins of the system. Treating these two terms separately allows greater flexibility and control in tuning the system response for each of the joint controllers while maintaining sufficient margins of stability.

The second important modification to the basic PID algorithm involves the addition of low-pass filtering to the derivative terms. Since the manipulator system does not include any sensors to directly measure joint velocities, these quantities must be calculated by taking the time-derivative of the measured joint positions. To prevent the amplification of high-frequency noise in the measured signal, a “low-pass derivative” operator is used to compute the joint velocities from the encoder measurements. This operator and the resulting modified PID algorithm are represented in the Laplace domain by Equations 2.10 and 2.11, respectively.

$$\dot{q} = \frac{100s}{s + 100} q_{measured} \quad (2.10)$$

$$\tau_{PID} = (K_P + K_{D1} \frac{100s}{s + 100} + \frac{K_I}{s})(q_{desired} - q_{measured}) + (K_{D1} - K_{D2}) \frac{100s}{s + 100} q_{measured} \quad (2.11)$$

The last important modification to the PID algorithm serves to reduce the effect of “integrator windup.” While tracking large and/or long motions, sustained tracking errors can cause the integral control term to become quite large. This can lead to excessive overshoot at the conclusion of these motions. To reduce this windup effect, a saturation limit is built into the calculation of the integral term as follows:

$$\int_t^{t+1} \Delta q dt = \left\{ \begin{array}{l} 0 \quad \text{if } K_I \int_0^t \Delta q dt = S \text{ and } \Delta q > 0 \\ 0 \quad \text{if } K_I \int_0^t \Delta q dt = -S \text{ and } \Delta q < 0 \\ \int_t^{t+1} \Delta q dt \quad \text{otherwise} \end{array} \right\} \quad (2.12)$$

This freezes the growth of the error integral when the magnitude of the integral control torque reaches a certain limit  $S$ . The saturation limits used in this design were found empirically and are given in Appendix B.

## 2.4.2 Gain Scheduling

The effective joint inertias are not constant. Rather, they change with both the manipulator's pose and the inertial parameters of the payload being manipulated. The effect of changing payloads is an issue of particular importance because this manipulator is required to work with a wide variety of payloads ranging in weight from 0 to 3000 lbs. This means that the joint dynamics can change radically from one manipulator task to the next. To accommodate the large range of payloads without altering the basic joint control architecture, the controller uses gain scheduling [Shamma, et al, 1990].

Gain scheduling requires that multiple complete sets of gains are developed for the PID joint controllers. For this design, each set of gains is tuned for use with a particular type of payload. Prior to operation with any payload, the manipulator's operator must identify the intended payload to the control system. The control system will then consult a database of predetermined PID gains and select the set of gains appropriate for that payload. This allows the joint controllers to provide a stable and relatively consistent response characteristic despite large changes in payload inertia between tasks.

## 2.4.3 Joint Modeling and Gain Tuning

To tune the response of each individual joint controller, an analytical model for each of the manipulator joints was created. Each joint was modeled independently as a simple planar rotational joint with an effective inertia  $J_i$ . This yields a second-order, SISO (single input, single output) system with the input being the torque applied to the joint ( $\tau_i$ ) and the output being the position of the joint ( $q_i$ ). Expected disturbances such as gravity, friction, and ship motions are not included in this model because the control system will compensate for the effects of these disturbances independently (refer to Chapter 3). The resulting system is illustrated in Figure 2.5.

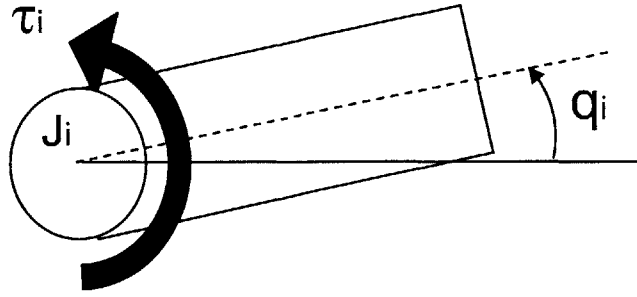


Figure 2.5. Joint model used in designing the PID joint controllers

The joint dynamics are expressed in the Laplace domain by the following transfer function.

$$\frac{q_i}{\tau_i} = \frac{1}{J_i s^2} \quad (2.13)$$

To calculate the effective joint inertias, a manipulator pose is chosen to represent a typical payload handling task. The manipulator dynamics are then modeled for this pose using the standard matrix form as defined by Equation 2.14 [Sciavicco, et al, 2000].

$$\mathbf{M}\ddot{\mathbf{q}} + \mathbf{C}(\mathbf{q}, \dot{\mathbf{q}})\dot{\mathbf{q}} + \mathbf{G}(\mathbf{q}) = \boldsymbol{\tau} \quad (2.14)$$

In the above formulation, the effective joint inertias  $J_i$  are the diagonals of the 6x6 inertia matrix  $\mathbf{M}$ . To make calculation of this inertia matrix less complex, the gravity vector and joint velocities can be set to zero. Equation 2.14 then reduces to the following form:

$$\mathbf{M}\ddot{\mathbf{q}} = \boldsymbol{\tau} \quad (2.15)$$

Finally, the Recursive Newton-Euler method [Sciavicco, et al, 2000] is applied to calculate the matrix  $\mathbf{M}$  and the diagonals are extracted to yield the effective joint inertias.

Having explicitly defined the transfer functions for the joint controllers and the joint dynamics, the joint control loop in Figure 2.4 can be updated as follows:

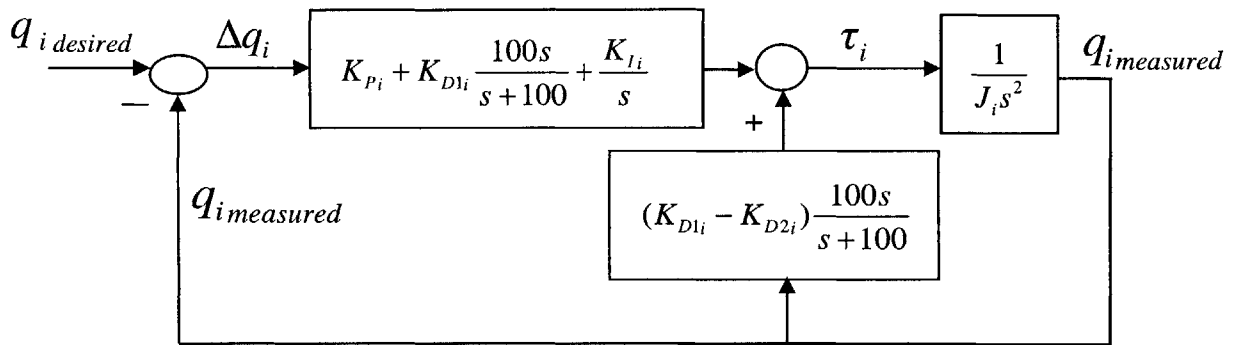


Figure 2.6. Joint control architecture with transfer functions defined

This joint control loop can be reduced and expressed as the following closed-loop transfer function relating the desired joint position  $q_{i\text{ desired}}$  to the measured joint position  $q_{i\text{ measured}}$ .

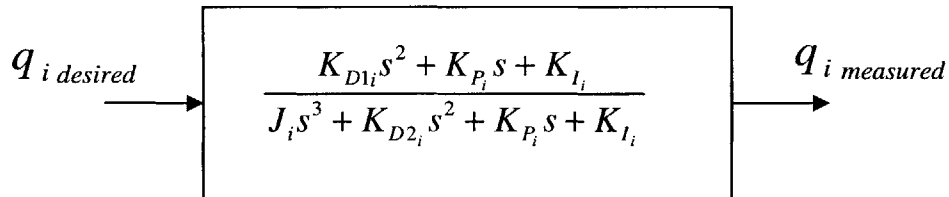


Figure 2.7. Reduced closed-loop transfer function for joint control

Now that the open-loop and closed-loop transfer functions have been defined, standard analysis tools can be applied to help find gains for the PID joint controllers that will yield the desired dynamic response [Astrom, 1995]. In the frequency domain, this includes the root locus, open-loop bode plot, and the closed-loop bode plot. In the time domain, analysis tools include the step-response and ramp-response. The root locus is used primarily to observe the damping ratio for the closed-loop response and also in conjunction with the open-loop bode plot to compute the stability margins. The closed-loop bode plot is used primarily to compute the bandwidth of the closed-loop system. The step-response and ramp-response were used to observe the characteristic responses of the closed-loop system to these input types.

Suitable gains for this system were found empirically while targeting two conditions. The first condition was a damping ratio of approximately 0.7 to provide a slightly under-damped response. It was decided that a modest amount of overshoot can be tolerated in exchange for giving the user the more responsive feel (i.e. faster rise time) that results from an under-damped design. The second condition was an upper limit for the controller's bandwidth determined by the manipulator's structural resonance properties. This limitation on bandwidth is discussed in greater detail in the next section.

The final joint controller designs have infinite gain margin and phase margins of 80-120 degrees. These stability margins are higher than is necessary for safety. This is a product of the strict bandwidth limitations imposed on the joint controllers by the structural resonance characteristics of the physical system. These bandwidth restrictions are the limiting factor in the joint controllers' performance.

#### **2.4.4 Structural Resonance and Controller Bandwidth**

Approximating the manipulator as a system of rigid links greatly simplifies the process of modeling and analysis. In reality, however, the manipulator is not a perfectly rigid system but rather a flexible system with multiple resonance modes. To guarantee the position controller's stability without including these resonance modes in the analysis model, the control system's bandwidth must be kept safely below the manipulator's

lowest resonance frequency [Townsend, 1972]. Limiting the bandwidth in this way guarantees that the control system cannot excite any of the manipulator's resonance modes.

The controller bandwidth is defined as the frequency at which the magnitude of the closed-loop transfer function drops below  $-3\text{dB}$ . The bandwidth essentially marks the upper limit of the controller's range of operational frequencies. To ensure stability, the controller must attenuate any command inputs at or near a resonance mode for the controlled system. A widely accepted rule of thumb states that a safe margin of stability can be ensured by limiting the controller's bandwidth to one "decade" (one order of magnitude) below the physical system's lowest structural resonance frequency [Book, 1974].

For the controller presented in this thesis, data was obtained from the manipulator's designer providing the system's structural resonance modes for operation with each of the payload types considered in this analysis. In tuning the PID joint control gains for each payload type, the bandwidth was placed approximately one decade below the manipulator's estimated lowest structural resonance mode for that payload. This ensures that the controller cannot excite any of the system's structural resonances during operation.

# CHAPTER 3

## **COMPENSATING FOR DISTURBANCES**

---

### **3.1 Introduction**

As discussed in Chapter 1, the most critical challenges in this control system design come from the large and generally unpredictable dynamic disturbances acting on the manipulator. These disturbances include, but are not limited to, the effects of gravity, base motions, and joint friction. As will be shown in Chapter 4, any one of these disturbances is enough to make the manipulator fail to meet its target specifications if not effectively compensated by the position control system.

The basic Cartesian and joint control architecture described in Chapter 2 does not attempt to model the effects of disturbances in the physical system. To estimate and compensate for these disturbances, therefore, it is necessary to include additional algorithms in the position control system. The function of these compensation algorithms is to counter the effects of any disturbances in the joints such that the manipulator behaves more like the purely linear system assumed in the design of the PID joint controllers. This chapter describes the various disturbance estimation and compensation methods used to perform this function.

### **3.2 Compensating for Gravity**

Of the various compensation challenges encountered in this design, compensating for gravity is the most straightforward. The solution uses a feed-forward approach that assumes full knowledge of the manipulator's kinematics, link masses (including payload),

and the gravity vector. Assuming zero joint velocities, the manipulator dynamics can be written as follows:

$$\mathbf{M}\ddot{\mathbf{q}} + \mathbf{G}(\mathbf{q}) = \boldsymbol{\tau} \quad (3.1)$$

where  $\mathbf{G}(\mathbf{q})$  is a 6x1 vector representing the joint torques due to gravity acting on the manipulator and its payload.

The vector  $\mathbf{G}(\mathbf{q})$  is calculated online either in closed-form or using the recursive Newton-Euler method. The static effects of gravity are then effectively canceled by reversing the signs of the torques in  $\mathbf{G}(\mathbf{q})$  and adding them to the commanded torques for each joint [Sciavicco, et al, 2000]. Figure 3.1 illustrates the flow of information involved in the gravity compensation process.

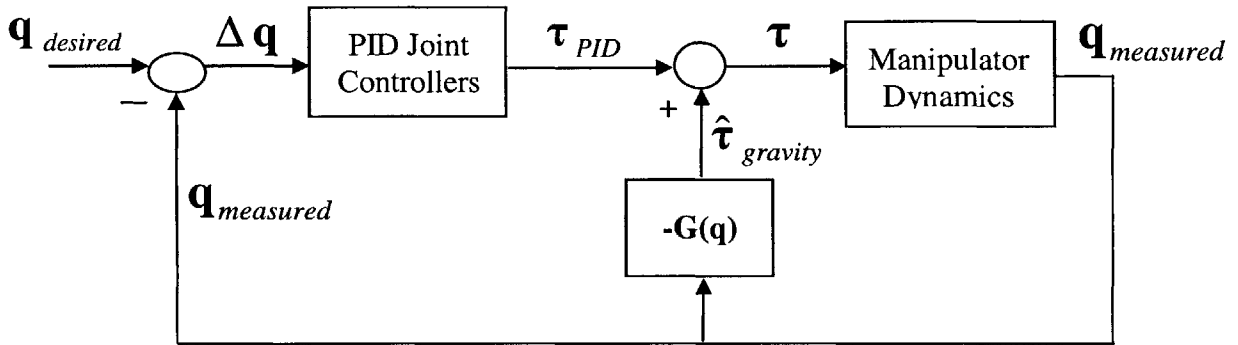


Figure 3.1. Joint control with feed-forward gravity compensation

$\hat{\boldsymbol{\tau}}_{gravity}$  is the 6x1 vector of computed gravity compensation torques. The accuracy of the gravity compensation depends on how accurately the manipulator's kinematic and mass parameters are known (payload included). If there are errors in these parameters, the computed compensation torques will not perfectly counteract the effects of gravity and this error will be seen as a disturbance in the system. It is therefore very important

that kinematic parameters of the manipulator and its payload are accurately known by the position controller.

### 3.3 Compensating for Ship Motions

As mentioned in Chapter 1, this position control system is designed for a manipulator operating on the deck of a large ship at sea. Because the manipulator's base is fixed to the ship's deck during operation, the motions experienced by the ship are likewise experienced by the manipulator. These base motions impart both translational and rotational accelerations on the manipulator and its payload. In addition, the rotational components of the motions cause the manipulator to rotate with respect to the gravity vector. If these rotations are not accounted for, large errors in the gravity compensation torques will result.

To compensate for the effects of ship motions, the control system uses the array of accelerometers and inclinometers in the manipulator's base to augment the gravity compensation algorithm described in the previous section [Sciavicco, et al, 2000, Agostini, et al, 2002, Love, et al, 2003]. The approach here is to model and compensate for the rotations and translational accelerations caused by ship motions exactly like the acceleration caused by gravity. Because this method uses a quasi-static model of the manipulator, it does not compensate for rotational accelerations, nor does it account for centripetal or coriolis effects. Fortunately, the manipulator operates exclusively on large ships where the rotational motions have relatively small amplitudes (< 13 degrees) and long periods (> 10 seconds). The uncompensated effects due to angular motions are not expected to be large enough to significantly degrade the performance of the position control system. This claim is validated by the simulation results presented in Chapter 4.

The compensation for ship motions is implemented by factoring the measured ship motions into the calculation of the gravity compensation torques. To begin, the gravity vector is pulled out of the vector  $\mathbf{G}(\mathbf{q})$  as follows:

$$\hat{\boldsymbol{\tau}}_{gravity} = -\mathbf{G}'(\mathbf{q})\mathbf{g} \quad (3.2)$$

where  $\mathbf{g}$  is the 3x1 gravity vector in the manipulator's base coordinates.

Inclinometers in the manipulator's base measure the pitch and roll of the manipulator relative to the world coordinates and rotate the gravity vector accordingly. Yaw motions are neglected because it is assumed that the ship will maintain a constant heading during manipulator operation and yaw motions due to sea state will be very small. The rotated gravity vector is represented as follows:

$$\hat{\boldsymbol{\tau}}_{gravity} = -\mathbf{G}'(\mathbf{q})\mathbf{R}(\theta_{pitch}, \theta_{roll})\mathbf{g} \quad (3.3)$$

where  $\mathbf{R}(\theta_{pitch}, \theta_{roll})$  is a rotation matrix that transforms the gravity vector from world coordinates to the manipulator's base.

Accelerometers in the manipulator's base measure the translational acceleration experienced due to the ship motions. This measured acceleration is then added to the rotated gravity vector as follows:

$$\hat{\boldsymbol{\tau}}_{gravity} = -\mathbf{G}'(\mathbf{q})(\mathbf{R}(\theta_{pitch}, \theta_{roll})\mathbf{g} + \mathbf{a}_{ship}) \quad (3.4)$$

where  $\mathbf{a}_{ship}$  is the 3x1 vector of translational ship accelerations measured in the manipulator's base coordinates.

To statically compensate for the combined effects of gravity and ship motions, the joint torques in  $\hat{\boldsymbol{\tau}}_{gravity}$  are fed-forward to the commanded joint torques as shown in Figure 3.2. In the ideal case where the manipulator/payload parameters and sensor measurements are 100% accurate, the compensation torques will perfectly cancel the effects of gravity and the translational accelerations caused by ship motions. Any errors

in the model parameters and/or sensor measurements, however, will affect the accuracy of the compensation torques and cause a dynamic disturbance in the system.

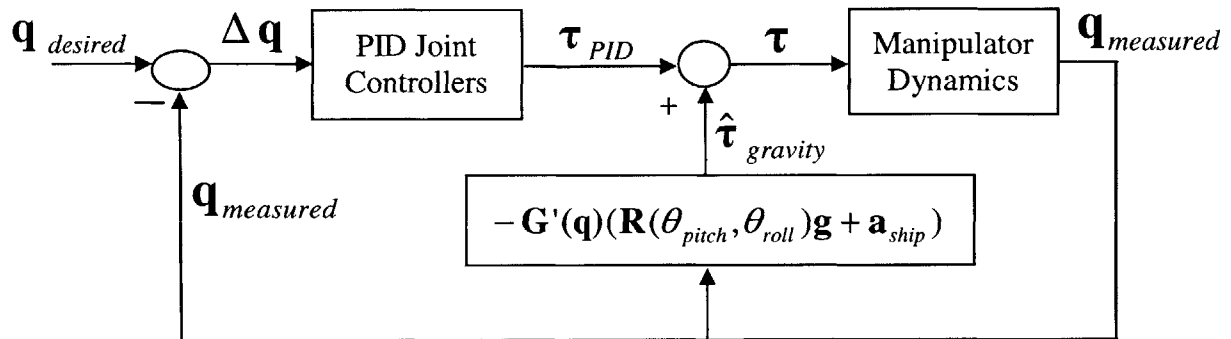


Figure 3.2. Joint control with feed-forward gravity and ship motion compensation

### 3.4 Modeling Joint Friction

It is important to have a good understanding of the joint friction in the system, both for simulating the physical system and for selecting a suitable compensation scheme. Understanding the joint friction means identifying the torque profile of the friction and which system variables, if any, are involved in its determination. This section describes the two basic friction models that are used to simulate joint friction in the manipulator. These models are approximations of the true friction behavior and are based on literature research [Dupont, 1993, Olsson, et al, 1998] and limited experimental data from the manufacturers of the manipulator system and mechanical components.

#### 3.4.1 Static-Load-Dependent Model (Joints 1-3)

The first three manipulator joints use transmissions to amplify the torque produced by their electric motors. It is assumed that the motor bearings and transmissions are the dominant sources of friction in these joints. Friction in the joint bearings is estimated to

be at least an order of magnitude lower than that in the motor bearings and transmissions and is therefore neglected in this analysis.

The transmissions for joints 1-3 include roller screws that convert the motor torques into linear forces (refer to Section 2.2). These screws are expected to produce coulomb friction that varies with the amount of load placed on the screws. As seen at the motor shaft, the friction from the screws is modeled as follows:

$$\tau_{screws} = -\alpha_1 F_{load} \operatorname{sgn}(\dot{q}) \quad (3.5)$$

where  $F_{load}$  is the static axial load on the roller screw,  $\dot{q}$  is the motor velocity, and  $\alpha_1$  is a constant.

The friction from the motor and the intermediate transmission is approximated by a constant coulomb term and a velocity-dependent viscous term as follows:

$$\tau_{motor+gear} = -(\alpha_2 + \alpha_3 |\dot{q}|) \operatorname{sgn}(\dot{q}) \quad (3.6)$$

where  $\alpha_2$  and  $\alpha_3$  are constants.

Without modeling any other effects, the total joint friction for joints 1-3 would thus be described by the following relationship:

$$\tau_{friction} = -(\alpha_1 F_{load} + \alpha_2 + \alpha_3 |\dot{q}|) \operatorname{sgn}(\dot{q}) \quad (3.7)$$

Based on prior research [Dupont, 1993], however, it was determined that the above linear representation of coulomb friction would be insufficient since it neglects a common and potentially significant nonlinear effect known as *stick/slip*. Stick/slip refers to the sudden nonlinear drop in coulomb friction that can occur when the contact surfaces transition from the “stick” condition (no relative motion) to the “slipping” condition

(relative motion). To model the stick/slip effect, the two coulomb friction terms in Equation 3.7 are multiplied by the nonlinear shaping function below [Armstrong, et al, 1994]:

$$S(\dot{q}) = \beta_1 + \beta_2 e^{-\beta_3 |\dot{q}|} \quad (3.8)$$

where  $\beta_1$ ,  $\beta_2$ , and  $\beta_3$  are constants that satisfy the conditions  $\beta_1 + \beta_2 = 1$  and  $\beta_3 > 0$ .

The resulting complete friction model for joints 1-3 is as follows:

$$\tau_{friction} = -[(\alpha_2 + \alpha_1 F_{load})S(\dot{q}) + \alpha_3 |\dot{q}|] \text{sgn}(\dot{q}) \quad (3.9)$$

The function  $S(\dot{q})$  is equal to unity at zero velocity, so the “breakaway” friction (i.e. the maximum friction at zero velocity) remains unchanged from Equation 3.7. As the velocity increases, however, the function decreases exponentially, simulating an overall reduction in the coulomb friction by  $(\beta_2 * 100)\%$ . This technique models a form of stick/slip behavior known as the *Stribeck* effect [Olsson, et al, 1998]. The general shape of this friction profile is illustrated in Figure 3.3 for a given static load  $F_{load}$ .

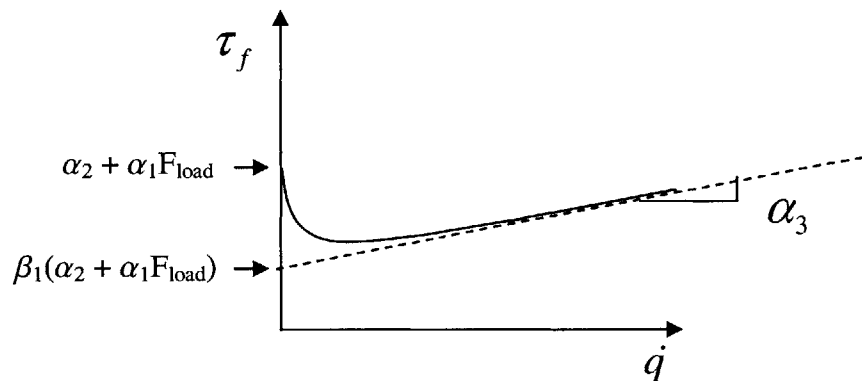


Figure 3.3. Stribeck effect in the static-load-dependent friction model

The parameters  $\alpha_1$ ,  $\alpha_2$ ,  $\alpha_3$ ,  $\beta_1$ ,  $\beta_2$ , and  $\beta_3$  are estimated using data from the manipulator's designer. The parameter values used in the analysis and simulation of this position controller are given in Appendix C.

### 3.4.2 Torque-Dependent Model (Joints 4-6)

Unlike the manipulator's first three joints, joints 4-6 use direct-drive motors and thus do not have transmissions. The only significant source of friction in these three joints is the motors themselves. The motors that drive joints 4-6 are very different in nature than those driving joints 1-3. These motors produce 100 to 1000 times more torque and are unique in design. The motor friction is therefore also unique and cannot be approximated by the same models used for joints 1-3.

Using experimental data provided by the motor designers, it was determined that the motor friction is dependent on three variables: joint velocity, commanded motor torque, and the peak-torque rating for the motor. From the data provided, it was determined that the total friction is best approximated by a linear dependence on joint velocity and a quadratic dependence on the commanded torque. In addition, the friction profile as a whole was found to scale linearly with the peak torque rating for the motor (joints 4-6 use differently sized versions of the same motor type). Additional nonlinear effects such as stick/slip did not appear to be significant from the data provided. Combining all three of these dependencies results in the following empirically-determined friction model:

$$\tau_{friction} = -(1 + \sigma_1 |\dot{q}|)(\sigma_2 + \sigma_3 |\tau_{motor}| + \sigma_4 \tau_{motor}^2) \text{sgn}(\dot{q}) \quad (3.10)$$

The values of the parameters  $\sigma_1$ ,  $\sigma_2$ ,  $\sigma_3$ , and  $\sigma_4$  for each joint were derived from the available motor data and are given in Appendix C.

## 3.5 Sensor-based Friction Compensation (Joints 1-3)

The control system compensates for friction in all six joints by using motor torques to counter the effects of friction. The effectiveness of this method directly depends on the controller's ability to identify the magnitude of the friction torque in each joint. The simulated friction models described in Section 3.4 are merely approximations of the expected friction derived from prior research and the limited experimental data available for this manipulator. These models cannot be relied upon to provide sufficiently accurate estimates of joint friction in the real system. For joints 1-3, the position controller instead relies on a system of sensors to help estimate the joint friction online during manipulator operation.

### 3.5.1 Friction Estimation Using Load Cells

As mentioned in Section 2.2, joints 1-3 are each actuated by electric motors acting through an intermediate transmission to turn a roller screw. Also recall that load cells are installed in each of the three roller screws at the ends furthest from the motors as illustrated in Figure 3.4. Each load cell measures the force at its location in the transmission.

If no mechanical losses occur between the motors and the load cells, then the forces at the load cells will equal the commanded motor torques multiplied by the gearing ratio (including the screw) as follows:

$$F_{Loadcell} = \tau_{motor} \frac{2\pi r}{L} \quad (3.11)$$

where  $r$  is the gear ratio of the intermediate transmission and  $L$  is the screw lead.

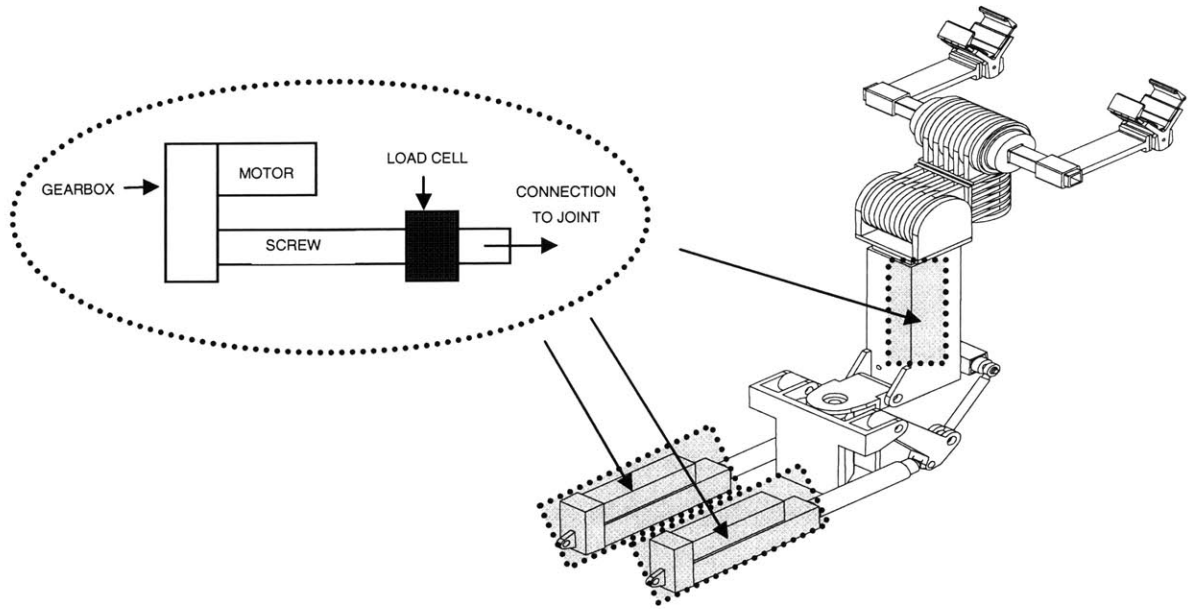


Figure 3.4. Location of load cells in joints 1-3  
(adapted from Foster Miller Inc.)

However, because there is friction in the system, the forces measured by the load cells will actually be reduced by some amount. Equation 3.11 thus becomes the following:

$$F_{Loadcell} = \tau_{measured} \frac{2\pi r}{L} = (\tau_{motor} - \tau_{friction}) \frac{2\pi r}{L} \quad (3.12)$$

$\tau_{measured}$  represents the amount of motor torque that is actually delivered through the transmission after the effects of friction. The difference between  $\tau_{motor}$  and  $\tau_{measured}$  is defined as  $\tau_{friction}$ .  $\tau_{friction}$  is assumed to be the total amount of motor torque lost to friction between the motor and the location of the load cell. Since all other quantities in Equation 3.12 are known or measured, this equation can be solved for the values of  $\tau_{measured}$  and/or  $\tau_{friction}$ .

It is important to note that the above technique only provides an estimate of the friction occurring from the load cell up to and including the motor. Any losses occurring

between the load cell and the joint itself (due to friction in the joint bearings, etc.) are outside the feedback loop and will not be detected. As previously stated, however, these losses are expected to be negligible compared to those experienced in the motors and transmissions.

### 3.5.2 Torque Control

Using the load cell measurements as feedback, torque control loops are formed around the motors and transmissions in joints 1-3 to compensate for the effects of friction [Luh, et al, 1983, Pfeffer, et al, 1989]. The torque controllers calculate the motor signal necessary to make the error between the desired torque and the measured output torque equal to zero. The form of the control loops is illustrated in Figure 3.5.

The torque controller uses a linear PI (proportional/integral) control law to drive the torque error to zero. Referring to the quantities defined in Figure 3.5, the torque control law is represented by the transfer function below:

$$\frac{\tau_{motor}}{\Delta\tau} = K_p + \frac{K_I}{s} = \frac{K_I \left( \frac{K_P}{K_I} s + 1 \right)}{s} \quad (3.13)$$

where  $K_p$  and  $K_I$  are constant gains different from those defined in Section 2.4.1.

The motor/transmission dynamics block in Figure 3.5 accounts for the loss of torque due to friction in these elements of the joint. For analysis, this torque loss can be represented as a disturbance affecting  $\tau_{motor}$ . The blocks representing the motor/transmission dynamics and the load cell sensor in Figure 3.5 can then be combined and reduced to yield the simplified block diagram shown in Figure 3.6.

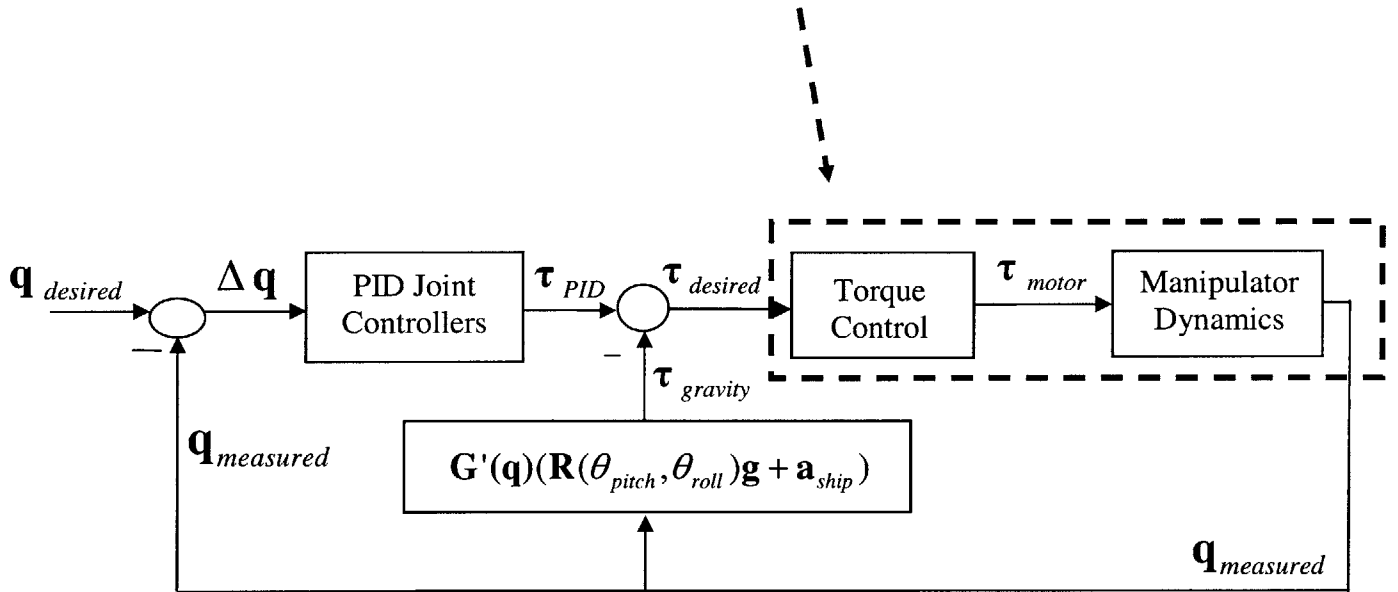
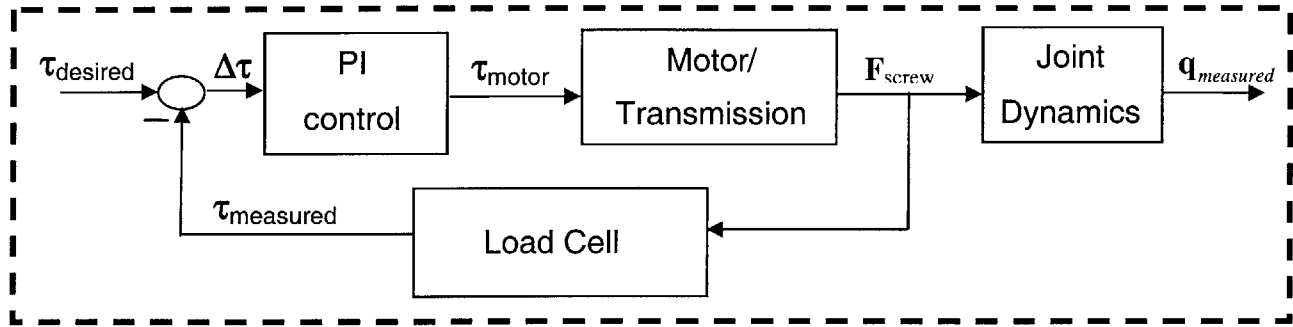


Figure 3.5. Torque control architecture (joints 1-3)

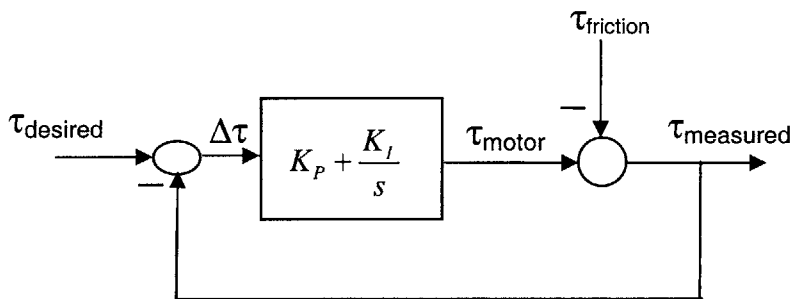
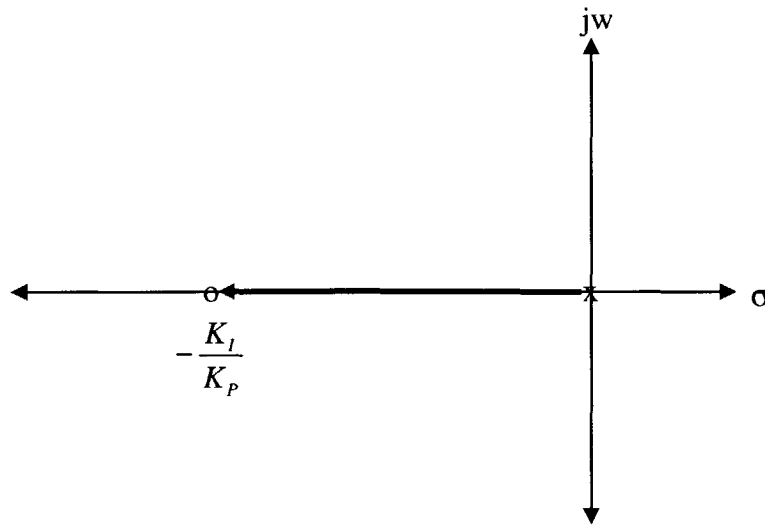


Figure 3.6. Simplified representation of the torque control architecture

Treating friction as a disturbance, the resulting closed loop transfer function for the torque controller is written as follows:

$$\frac{\tau_{measured}}{\tau_{desired}} = \frac{K_p s + K_I}{(K_p + 1)s + K_I} \quad (3.14)$$

The root locus for the open-loop system is shown in Figure 3.7. The torque controllers are stable for positive values of  $\frac{K_I}{K_p}$ . Increasing the gain raises the controller bandwidth. The system is first-order and well-behaved.



*Figure 3.7. Root locus for the PI torque controllers*

The joint controllers were designed in Chapter 2 without regard to the dynamics of these inner torque control loops. For the design of the joint controllers to remain valid, therefore, it is necessary that the torque control loops operate at a sufficiently higher bandwidth than the joint controllers. This will ensure that the torque control dynamics are effectively “invisible” to the joint controllers. Here, the torque control gains  $K_p$  and

$K_i$  were selected to give the torque controllers a bandwidth approximately ten times higher than that of the joint position controllers. The gain values used in simulation are listed in Appendix B.

### 3.6 Adaptive Friction Compensation (Joints 4-6)

Joints 4-6 do not have torque sensors installed and thus cannot rely upon a sensor-based friction compensation scheme. Instead, an adaptive algorithm is used to estimate and compensate for the friction in these joints. The adaptive estimation allows the position controller to estimate the magnitude of the joint friction online and in real-time. This is done without any sensors or predetermined model parameters for the joint friction. As a result, the adaptive estimation is robust to un-modeled effects and changes in the friction parameters over time.

The adaptive algorithm used to estimate joint friction in joints 4-6 was originally proposed by Friedland and Park for the purpose of identifying friction in mechanical joints [Friedland, et al, 1992]. This method has been shown in several different works to provide accurate online estimation of friction in position control systems [El-Roy, et al, 1995, Amin, et al, 1997, Kim, et al, 2002]. Like most adaptive algorithms, the Friedland-Park algorithm is based around a dynamic model of the joint. The joint model assumed in the formulation of this method is shown in Figure 3.8. In this model, the total torque acting on the joint is the sum of an applied torque  $\tau_{i,applied}$  and a disturbance torque  $\tau_{i,friction}$ . The effects of gravity and ship motions are ignored in this formulation because they are assumed to be compensated for independently.

The function of the Friedland-Park algorithm is to identify the magnitude of the disturbance  $\tau_{i,friction}$ . It is assumed for analysis that  $\tau_{i,friction}$  is entirely the result of joint friction. In reality, this torque may also include small contributions from random disturbances (wind, etc.) and errors in the gravity and ship motion compensation. As will be discussed later in this section, the presence of these additional uncompensated

disturbances can confuse the adaptive estimators and cause their output to misrepresent the true joint friction.

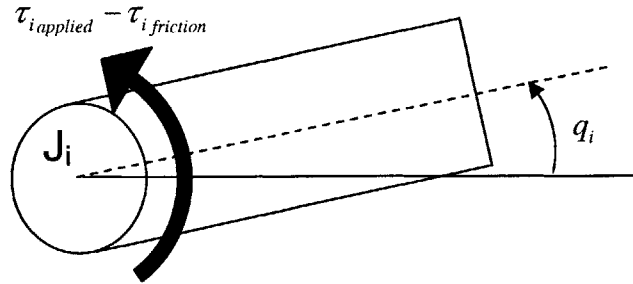


Figure 3.8. Joint model for the formulation of the Friedland-Park estimation method

The Friedland-Park algorithm assumes that  $\tau_{i\ friction}$  is the instantaneous friction torque acting on the joint. This torque is modeled as a variable magnitude  $a_i$  multiplied by the sign of the joint velocity as follows:

$$\tau_{i\ friction} = a_i \operatorname{sgn}(\dot{q}_i) \quad (3.15)$$

It is assumed that  $\tau_{i\ applied}$  is the torque applied through the motor by the position control system (minus gravity and ship motion compensation). This applied torque consists of two terms: the PID control torque plus a friction compensation torque as shown below.

$$\tau_{i\ applied} = \tau_{i\ PID} + \hat{\tau}_{i\ friction} \quad (3.16)$$

The friction compensation torque  $\hat{\tau}_{i \text{ friction}}$  is the adaptive estimator's current estimate of the instantaneous joint friction  $\tau_{i \text{ friction}}$ . Following the form of Equation 3.15, this torque is written as follows:

$$\hat{\tau}_{i \text{ friction}} = \hat{a}_i \text{sgn}(\dot{q}_i) \quad (3.17)$$

The instantaneous joint friction is therefore estimated for each joint  $i$  by identifying the single parameter  $\hat{a}_i$  which is an estimate of the friction magnitude  $a_i$  in Equation 3.15. The function of the adaptive algorithm is to compute the estimates  $\hat{a}_i$  in real time during manipulator operation. Using these estimates, the friction compensation torques  $\hat{\tau}_{i \text{ friction}}$  for joints 4-6 are computed and fed-forward into the commanded motor torque to counteract the effects of joint friction.

The estimate  $\hat{a}_i$  is computed in real time using the following adaptation law:

$$\hat{a}_i = z_i - J_i k_i |\dot{q}_i|^{\mu_i} \quad (3.18)$$

$$\dot{z}_i = k_i \mu_i |\dot{q}_i|^{\mu_i - 1} [\tau_{i \text{ applied}} - \hat{\tau}_{i \text{ friction}}] \text{sgn}(\dot{q}_i) \quad (3.19)$$

where  $J_i$  is the effective joint inertia,  $k_i$  and  $\mu_i$  are positive gains selected by the designer, and  $z_i$  is an intermediate variable.

By substitution of Equations 3.16 and 3.17, Equation 3.19 reduces to the following:

$$\dot{z}_i = k_i \mu_i |\dot{q}_i|^{\mu_i - 1} \tau_{i \text{ PID}} \text{sgn}(\dot{q}_i) \quad (3.20)$$

Figure 3.9 shows the joint control architecture with adaptive estimation and compensation for joint friction.

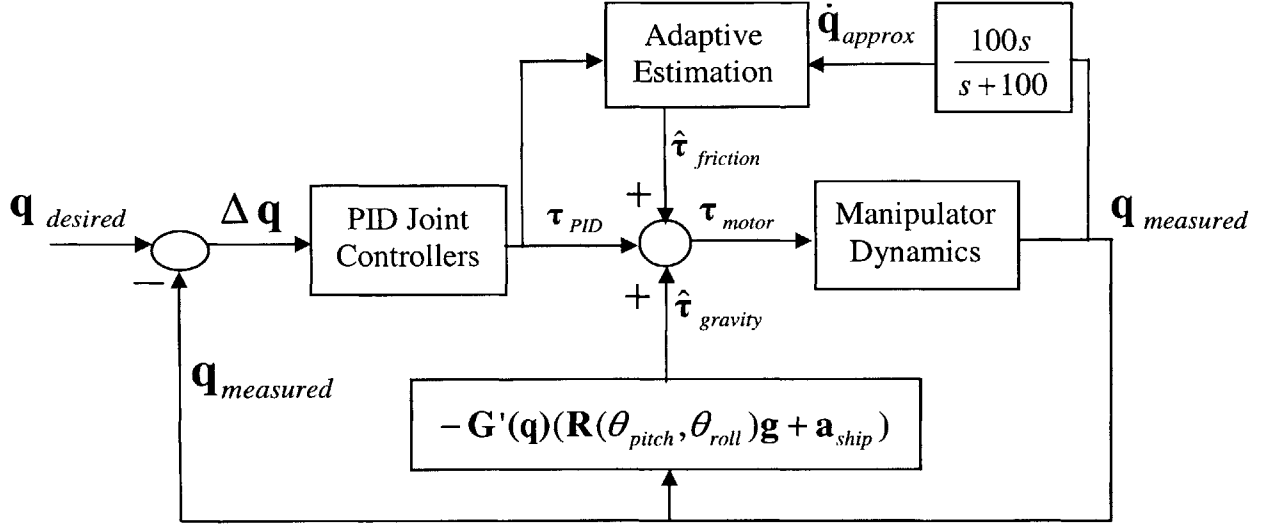


Figure 3.9. Joint control architecture with adaptive friction estimation and compensation

The proof of convergence for the Friedland-Park algorithm employs the Lyapunov theorem and can be found in the reference materials [Friedland, et al, 1992]. The important result of this proof is that the estimation error  $e_i \equiv \hat{a}_i - a_i$  converges to zero according to the following equations:

$$e_i = a_i - \hat{a}_i \quad (3.21)$$

$$\dot{e}_i = \dot{a}_i - k_i \mu_i |\dot{q}_i|^{\mu_i - 1} e_i \quad (3.22)$$

This result guarantees that the estimate  $\hat{a}_i$  will continue to track the true value  $a_i$  with zero steady-state error provided there is sufficient excitation of the joint (i.e.  $\dot{q}_i > 0$ ). The amount of joint excitation required for satisfactory convergence is a function of the gains  $k_i$  and  $\mu_i$ . The practical limits on these gains vary with each joint. The values used for  $k_i$  and  $\mu_i$  in this system were determined empirically in simulation by observing compensator performance and are given in Appendix B.

As previously mentioned, the adaptive estimator does not distinguish between disturbance torques caused by joint friction and disturbance torques from any other

source. The joint model simply assumes that any joint torque that is not accounted for in  $\tau_{i_{applied}}$  is due to friction. As a result, any additional uncompensated disturbances (due to wind, errors in the gravity compensation, etc.) are perceived as friction and included in the friction estimate. This is advantageous in the sense that the additional disturbances are consequently compensated for along with the joint friction. The disadvantage, however, is that the inclusion of these additional torques can cause the friction estimates to misrepresent the true joint friction. As will be discussed in the following section, this can present a problem when the manipulator contacts the environment and the adaptive estimation must be turned off.

### **3.7 Contact Forces and Friction Model Extraction**

Disturbances such as friction and gravity are finite and thus can be counteracted by applying equal and opposite torques to the joints. This is not necessarily the case with disturbances that result from the manipulator coming into contact with the environment. Certain objects in the manipulator's environment are assumed to be rigid and therefore no amount of force will allow the manipulator to pass through these objects.

As discussed in Section 3.6, the adaptive estimators on joints 4-6 do not distinguish between joint friction and other uncompensated disturbances. The adaptive compensation will perceive the contact forces as additional joint friction and attempt to compensate. As a result, the friction estimates generated by the adaptive estimators will no longer represent the true joint friction. Furthermore, the adaptive compensation will effectively try to force the manipulator through the object it is in contact with, commanding an infinitely increasing amount of torque from the joint motors.

To prevent this scenario from occurring, adaptive estimation must be temporarily deactivated during portions of manipulator operation that require contact with the environment. During these intervals, the control system switches to a feed-forward method of friction compensation for joints 4-6 using a temporary estimated model of the friction as shown in Figure 3.10. This can also be done for joints 1-3, although it is not fundamentally necessary.

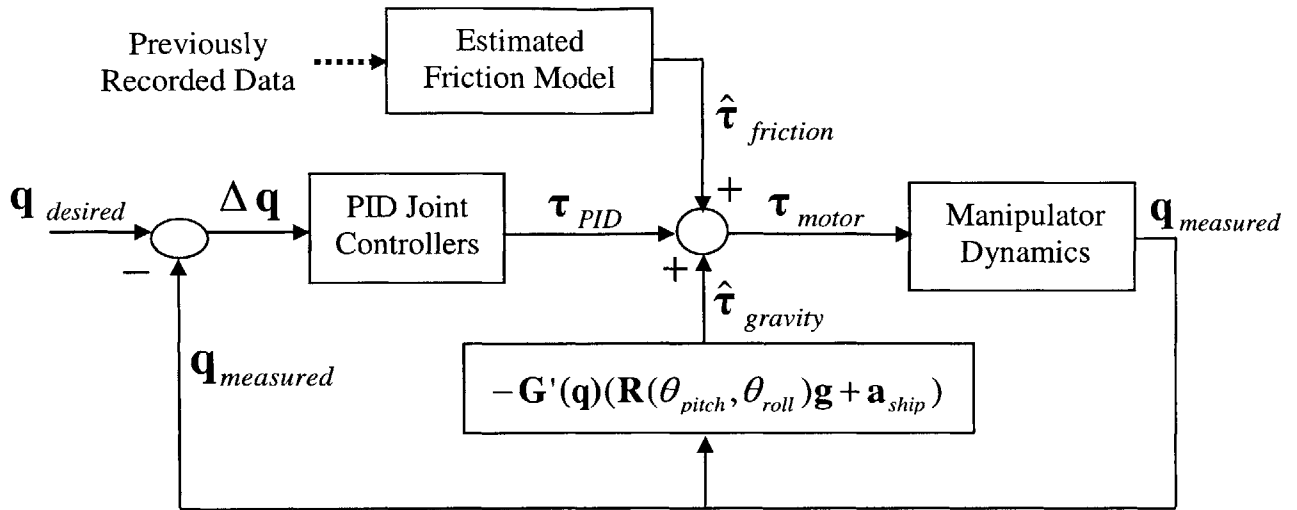


Figure 3.10. Joint control with feed-forward friction compensation using models extracted from estimator data

The general form of the estimated friction models is predetermined, but the exact parameter values are not. Instead, the parameter values for the model are identified for each joint online using recorded friction estimates  $\hat{\tau}_{friction}(t)$  from the adaptive estimators (or torque controllers). New parameters may be identified each time the adaptive estimators are deactivated, discarding the previous models. This ensures that the feed-forward friction models always reflect the most recently observed dynamics.

The process of extracting a joint friction model requires recorded estimates of the friction magnitude and any independent variables that appear in the assumed model. Independent variables are limited to those that are either known or measured by the system during operation ( $q$ ,  $\dot{q}$ ,  $\tau_{motor}$ , etc.). The parameters of the model are then identified by performing a curve-fit of the recorded data to the assumed form of the friction model. Section 4.3.6 presents an example of this procedure for joint 6 using simulation data.

## 4.1 Introduction

System hardware was not available for testing at the time of this thesis. The performance of the position controller was instead evaluated through extensive modeling and simulation. This chapter presents the results of various simulation studies that examine the controller's ability to track commanded motions in representative operational scenarios.

## 4.2 Simulation Setup

The mechanical system is simulated by a dynamic model of the manipulator constructed in MSC.ADAMS<sup>®</sup>. This dynamic model contains the geometry and inertial parameters for the manipulator and a given payload based on the available manipulator design data. The model should therefore accurately represent the kinematics and basic inertial dynamics of the real system. The model also includes a gravity field that is used to simulate the effects of gravity and ship motions.

The position control system is modeled in Simulink<sup>®</sup>. To simulate manipulator control, a desired path is generated for the manipulator's end-effector. This path can be of the form  $\mathbf{X}_{desired}(t)$  (for Cartesian control) or  $\mathbf{q}_{desired}(t)$  (for direct joint control), or it may contain segments of both forms. The time-derivative of this path is given to the control model to simulate a series of velocity command inputs from the operator. During simulation, the control system model computes the joint torques  $\boldsymbol{\tau}(t)$  necessary to

produce the end-effector path corresponding to these velocity commands. The nonlinear dynamic equations generated from the ADAMS manipulator model take the joint torques as inputs and return the resulting joint motions. This process is illustrated in Figure 4.1.

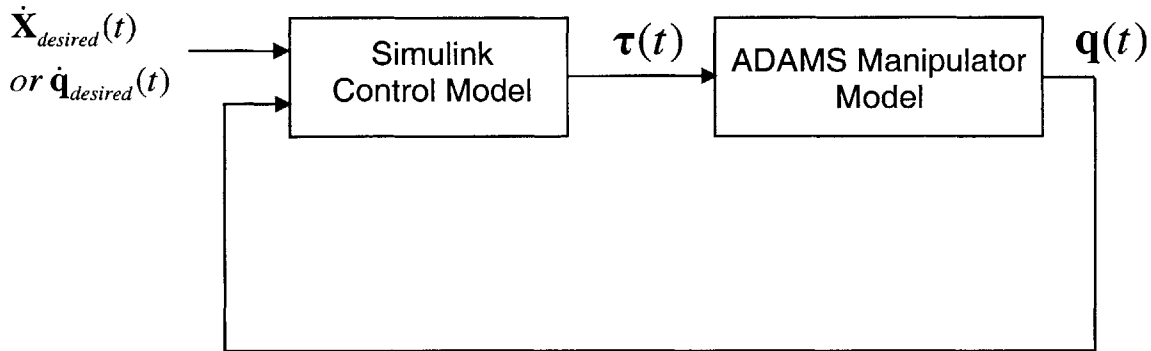


Figure 4.1. Structure of the position control simulation process

Because the ADAMS manipulator model does not include the effects of joint friction, friction must be calculated within the Simulink model and factored into the output torque  $\boldsymbol{\tau}(t)$ . The friction torque for each of the joints is calculated using the models described in Sections 3.4.1 and 3.4.2. The computed friction torque is then added to the output of the position controller to produce  $\boldsymbol{\tau}(t)$ . The result is that the effects of joint friction are included in the output torque  $\boldsymbol{\tau}(t)$ .

**Unless otherwise specified,** the studies presented in this Chapter make the following modeling assumptions:

1. The geometric and inertial parameters of the manipulator and its payload are exactly known by the position controller.
2. All sensor measurements are 100% accurate and noise-free.
3. All simulated command inputs  $\dot{\mathbf{X}}_{desired}(t)$  are smooth (i.e. contain no discontinuities or high-frequency inputs).
4. The manipulator does not make contact with any objects in the environment.

5. There is no simulated ship motion.
6. Joint motors deliver commanded torques perfectly and instantaneously (“torque ripple” effects are neglected).

## **4.3 Simulation Results**

### **4.3.1 Representative Heavy-Payload Task**

The manipulator system is designed for a maximum operational payload of 3000 lbs. This payload represents a critical challenge for the position control system for two reasons. First, the large payload mass lowers the structural resonances of the mechanical system and consequently the joint controllers are limited to a lower bandwidth for this payload than for any other payload. Second, the friction magnitudes in all joints increase as the payload mass increases and thus are at a maximum for this payload. For these reasons, the 3000 lb payload represents a type of “worst case” condition for the position control system. An important step in validating the design of the position controller is to show that the target performance specifications for this scenario can be met.

Using input from the designers of the mechanical system, a Cartesian trajectory was derived to represent the commanded motions of the manipulator’s end-effector during a typical 3000 lb payload task. The representative commands include payload repositioning and vertical insertion of the payload into a hole. Figure 4.2 shows the path that the end-effector is commanded to follow relative to the manipulator’s base coordinate system.

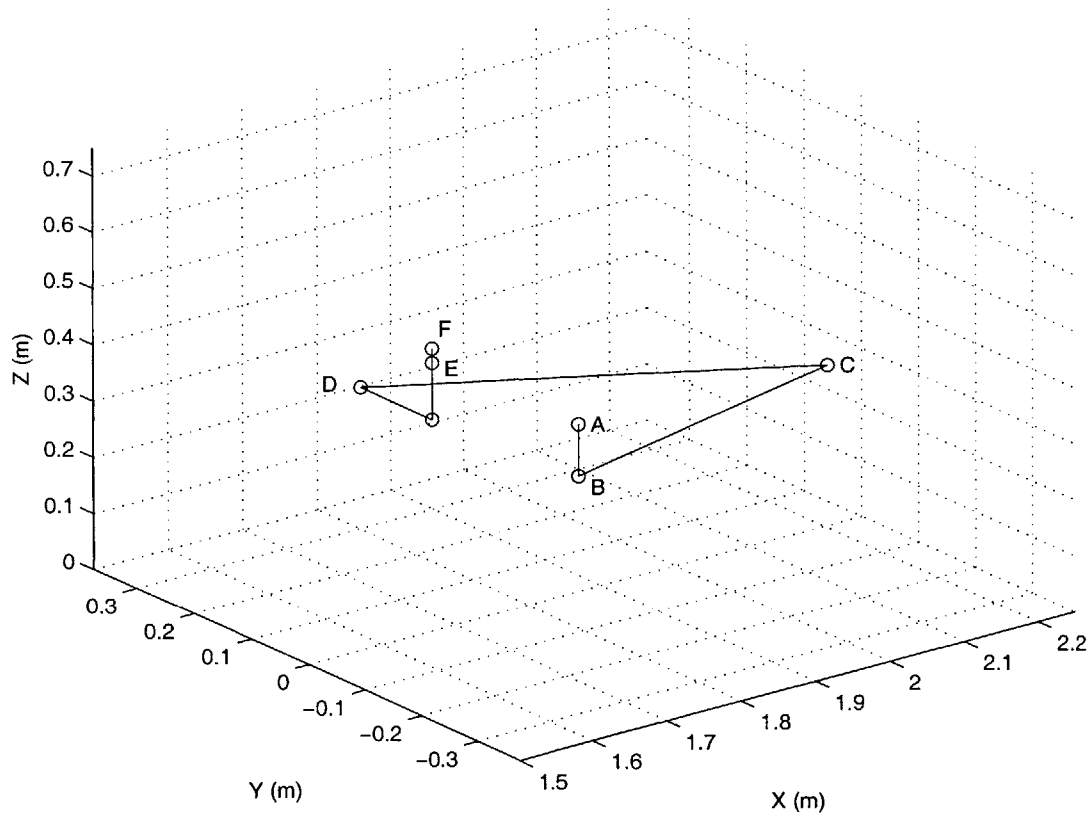


*Figure 4.2. End-effector trajectory in base-coordinates for the representative heavy-payload task*

The sequence of manipulator motions for the representative heavy-payload task is described as follows:

- **A:** Starting position. Manipulator is extended horizontally. Joint 5 is at a  $30^\circ$  angle to avoid a singular configuration.
- **A $\rightarrow$ B:** Payload is lowered approximately 0.1 meters vertically in 2 seconds.
- **B $\rightarrow$ C:** Payload is translated diagonally up and to the side (approximately 0.6 meters total). 8 seconds of motion followed by 2 seconds of settling time.
- **C $\rightarrow$ D:** Joint 5 is rotated  $60^\circ$  (axis of joints 4 and 6 are now perpendicular). 8 seconds of motion followed by 2 seconds of settling time.

- **D→E:** Payload is translated laterally 0.127 meters (5 inches) in 4 seconds and then raised vertically 0.102 meters (4 inches) in 4 seconds followed by 2 seconds of settling time.
- **E→F:** Payload is raised an additional 0.025 meters (1 inch) vertically. 5 seconds of motion followed by 4 seconds of settling time.

The target performance specifications for the position controller during the heavy-payload task are as follows:

*Table 4.1. Target performance specifications for the representative heavy-payload task*

	<u>Max. Translational Error</u>	<u>Max. Orientation Error</u>
Motions A – E:	2.5 cm	5°
Motion E – F (insertion):	1.0 cm	1°

The time-derivative of the representative heavy-payload trajectory was input to the position control model and a full dynamic simulation was run with a 3000 lb payload attached at the end-effector. Figure 4.3 shows the Cartesian tracking error as the position controller tracked the trajectory in simulation.

The Cartesian tracking results for the representative heavy-payload task are summarized below:

*Table 4.2. Tracking error results for the representative heavy-payload task*

	<u>Peak Translational Error</u>	<u>Mean Translational Error</u>
Motions A – E:	2.28 cm	-
Motion E – F (insertion):	0.45 cm	-
All Motions:	2.28 cm	0.7 cm

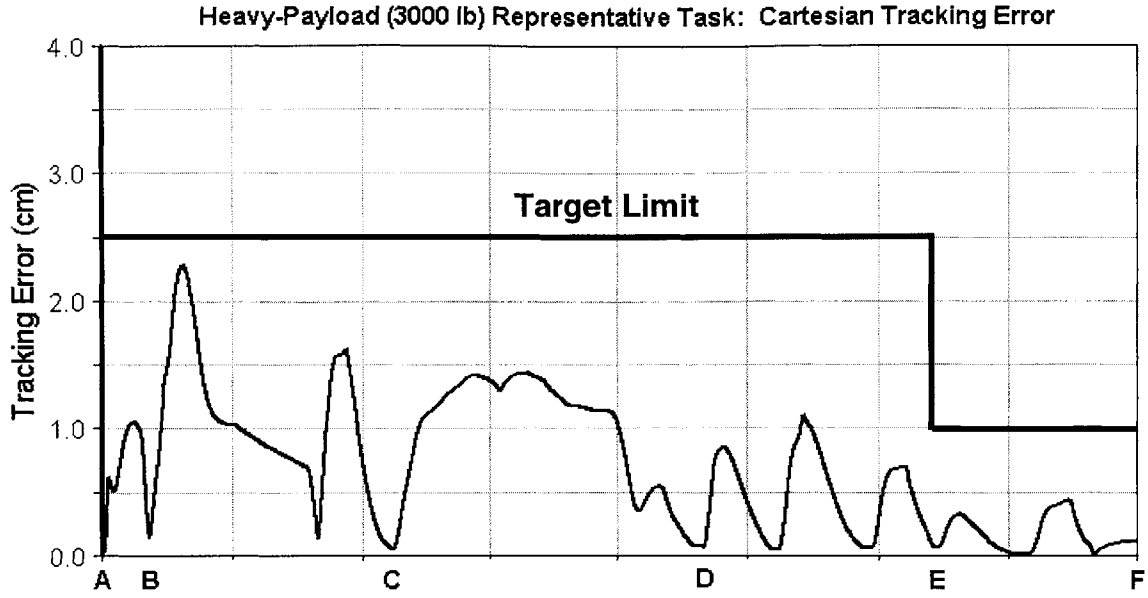
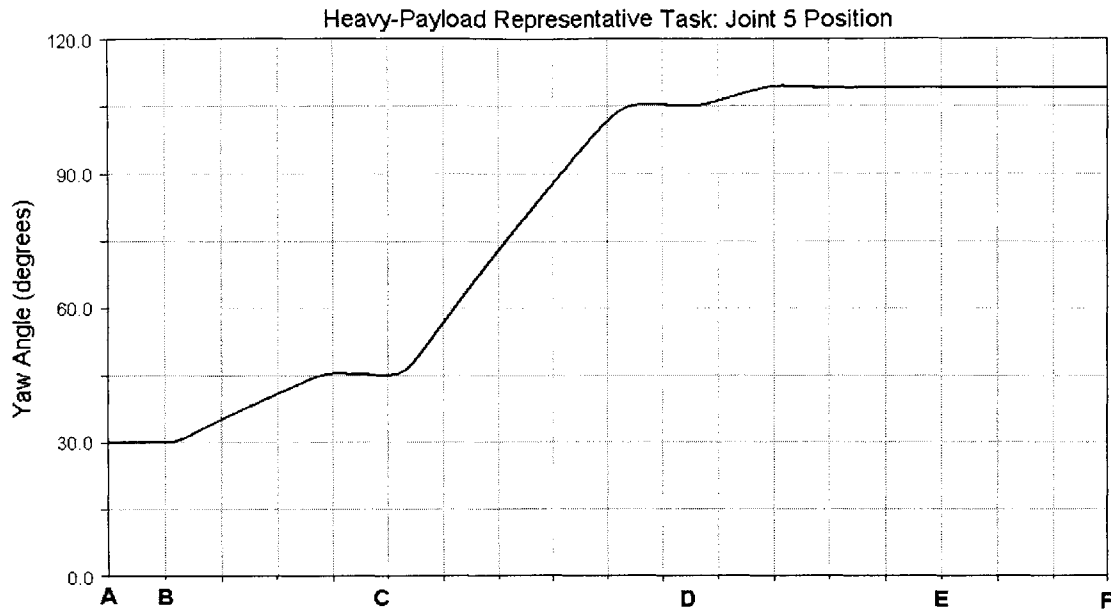


Figure 4.3. Translational end-effector tracking error during the representative heavy-payload task

The largest tracking error prior to position E is 2.28 cm, occurring during the large lifting motion between positions B and C. This falls within the target maximum limit of 2.5 cm for this portion of the task. The peak tracking error during motion E→F (payload insertion) is less than 0.5 cm. This falls within the target limit of 1.0 cm for this motion. The position controller meets the target performance specifications on the Cartesian tracking error for this task.

The only significant orientation error during this simulation occurs about the end-effector's yaw axis during motion C→D. The only joint involved in this motion is joint 5 and the angular tracking error during the task is dominated by the position error in this joint. Figure 4.4 shows the angle of joint 5 throughout the simulated task. The peak angular tracking error is less than 1°, which is well within the target limit for this task.



*Figure 4.4. Position of joint 5 during the representative heavy-payload task*

To demonstrate the effectiveness of the friction compensation employed by the position controller, two simulations were run with the same trajectory. In one simulation, friction was completely removed from the simulated manipulator dynamics. In the other simulation, friction remained in the simulated dynamics but all friction compensation was removed. The resulting Cartesian tracking error for all three simulations is shown in Figure 4.5.

As these results show, the friction compensation allows the mechanical system to behave very nearly like a frictionless system. Without compensation, however, joint friction in the system causes a dramatic reduction in tracking performance, increasing the Cartesian error by nearly a factor of 10 in some parts of the trajectory and exceeding the target limit. This result demonstrates the critical importance of effective friction compensation in the successful operation of this system.

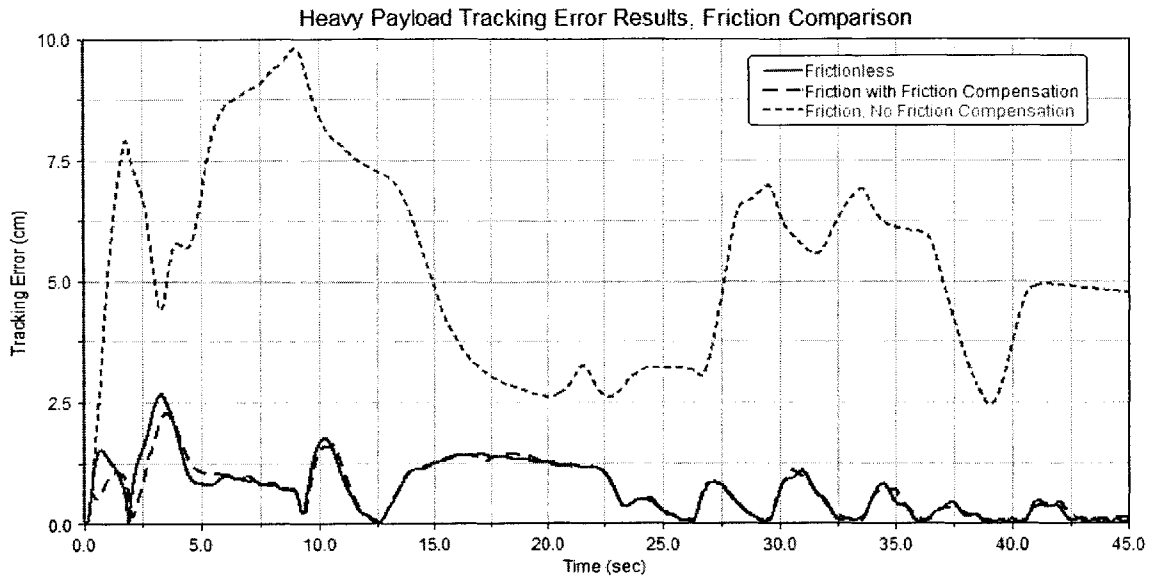
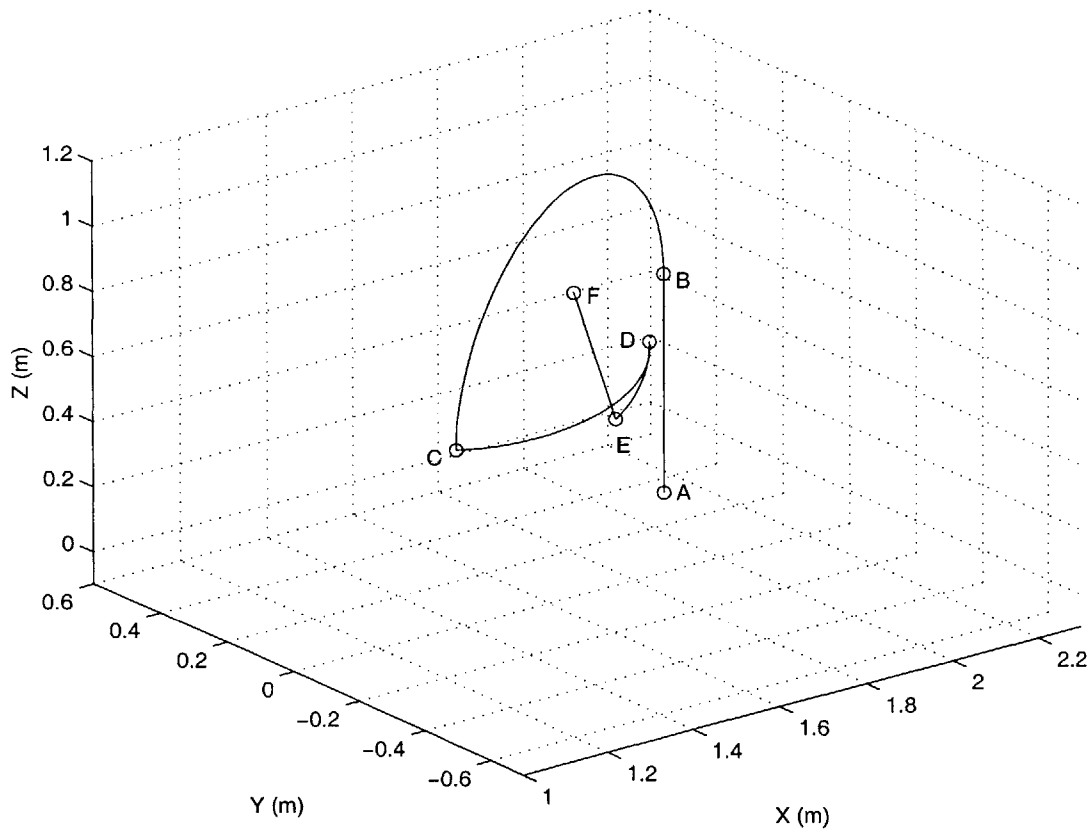


Figure 4.5. Comparison of tracking error with and without friction compensation

### 4.3.2 Representative Light-Payload Task

While the manipulator is rated for payloads up to 3000 lbs, the majority of its operational time will be spent working with lighter payloads ranging in mass between 100-400 lbs. To study this type of “light-payload” task, input from the system designers was used to define a second representative trajectory consisting of typical task motions for a payload in this range. This representative trajectory involves only payload repositioning (i.e. no insertion motion). The path that the end-effector is commanded to follow for the light-payload representative task is shown below in the manipulator’s base coordinate system.



*Figure 4.6. End-effector trajectory in base-coordinates for the representative light-payload task*

The sequence of manipulator motions for the representative light-payload task is described as follows:

- **A:** Starting position. Manipulator is extended horizontally. Joint 5 is at a  $30^\circ$  angle to avoid a singular configuration.
- **A→B:** Payload is raised vertically approximately 0.75 meters (25 inches) in 5 seconds followed by 2 seconds of settling time.
- **B→C:** Joint 6 is rotated  $180^\circ$  under direct joint control in 25 seconds followed by 1 second of settling time.
- **C→D:** Joint 5 is rotated  $45^\circ$  and joint 1 is rotated simultaneously  $15^\circ$  under direct joint control. (joint 6 is now parallel to the X axis). 9 seconds of motion followed by 1 second of settling time.

- **D→E:** Joint 6 is rotated 30° under direct joint control in 5 seconds followed by 1 second of settling time.
- **E→F:** Payload is simultaneously raised 0.33 meters (13 inches) vertically and translated 0.127 meters (5 inches) laterally under Cartesian control. 5 seconds of motion followed by 2 seconds of settling time.

The target performance specifications for the position controller during the light-payload task are stated in Table 4.3.

*Table 4.3. Target performance specifications for the representative light-payload task*

	<u>Max. translational error</u>	<u>Max. orientation error</u>
All Motions:	2.5 cm	5°

The time-derivative of the representative light-payload trajectory was input to the position control model and a full dynamic simulation was run with a 344 lb payload mass attached at the end-effector. Figure 4.7 shows the Cartesian tracking error as the position controller tracked the representative light-payload trajectory in simulation.

The Cartesian tracking results for the representative light-payload task are summarized in Table 4.4.

*Table 4.4. Tracking error results for the representative light-payload task*

	<u>Peak Translational Error</u>	<u>Mean Translational Error</u>
All Motions:	1.52 cm	0.32 cm

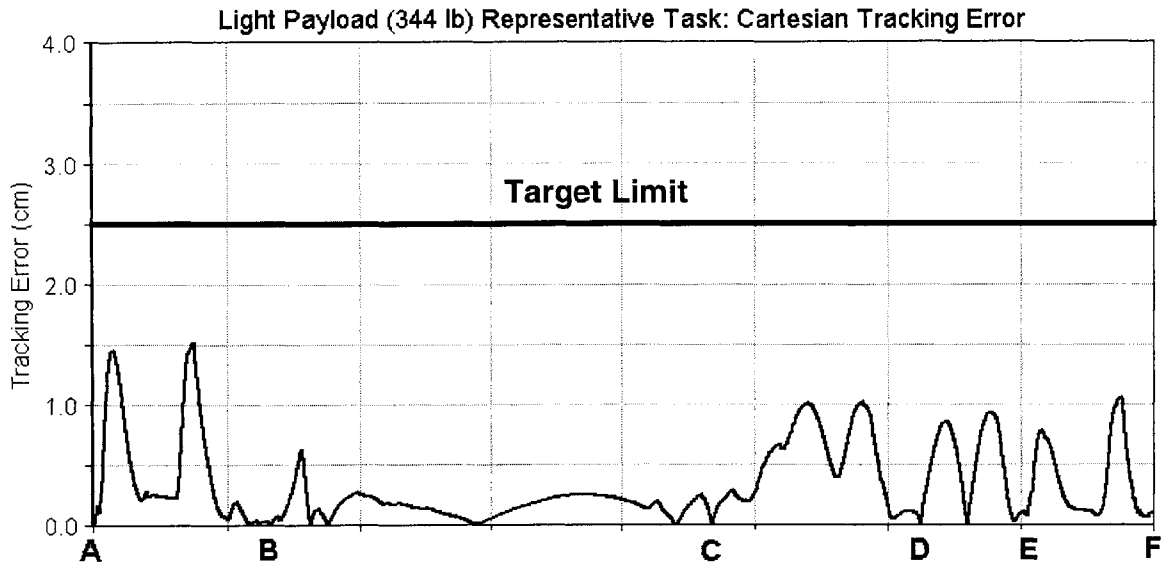


*Figure 4.7. Translational end-effector tracking error during the representative light-payload task*

The peak Cartesian tracking error is 1.52 cm occurring during the initial 75 cm vertical motion. This is a particularly difficult motion because it requires large movements from multiple joints at once. It is reasonable to expect large tracking errors from the position controller during this motion. Even so, the controller's performance meets the target specifications on Cartesian tracking error for this task.

The dominant sources of angular tracking error during this task are the joint rotations occurring between positions B and E. These motions involve joints 1, 5, and 6 only. The angles of these joints throughout the task are shown in Figure 4.8. The peak joint error is  $1.04^\circ$ , occurring in joint 6 during motion B→C approximately 47 seconds into the task. This is well within the target limit for angular tracking error in this task.

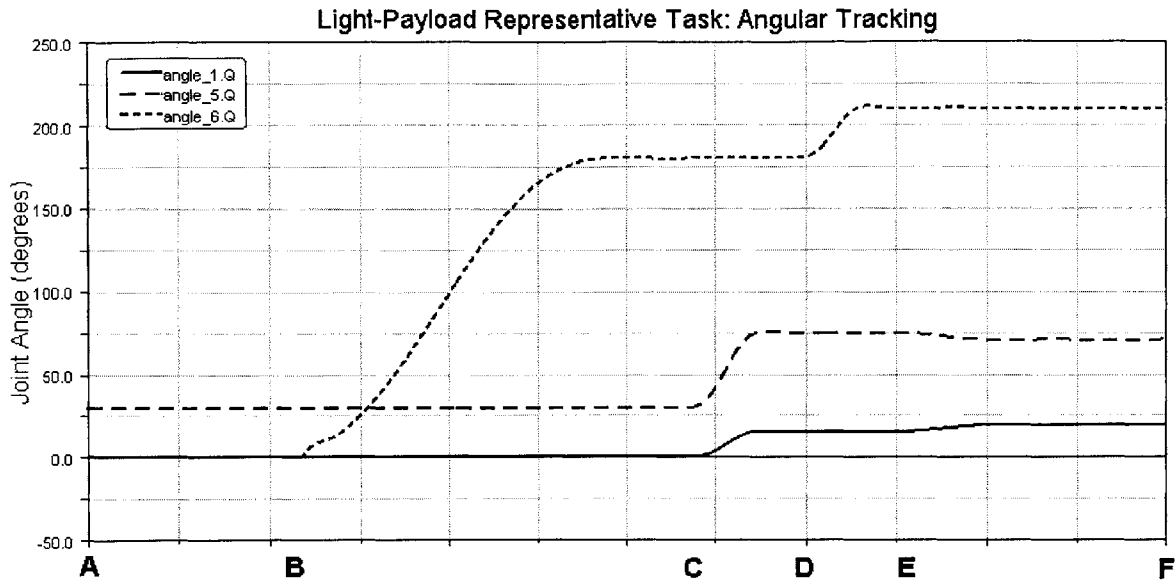


Figure 4.8. Position of joints 1, 5, and 6 during the representative light-payload task

### 4.3.3 Resolution Study

In the context of manipulator control, *resolution* is a metric of the smallest commanded motion that the position controller can respond to with sufficient accuracy. Resolution is particularly important for this system due to the limits of human operators. It will be virtually impossible for a human operator to supply the perfect commands to complete each desired motion in a single move, as is done in simulation. In reality, the first set of inputs for a given motion will likely only get the manipulator close to the desired position. The operator will then need to command one or more small adjustments to place the manipulator at the exact desired position. It will therefore be important that the position control system have sufficient resolution to make such small corrective motions possible.

A simulation study was conducted to test the position controller's ability to track commanded translations 1 cm in magnitude. The position controller was given an end-effector trajectory consisting of a 0.15 Hz square wave along the Y axis in base coordinates. A simulation was then performed with a 344 lb payload attached at the end-

effector. For comparison, the same simulation was the repeated with friction compensation deactivated. The lateral tracking error for both simulations is shown in Figure 4.9 below.

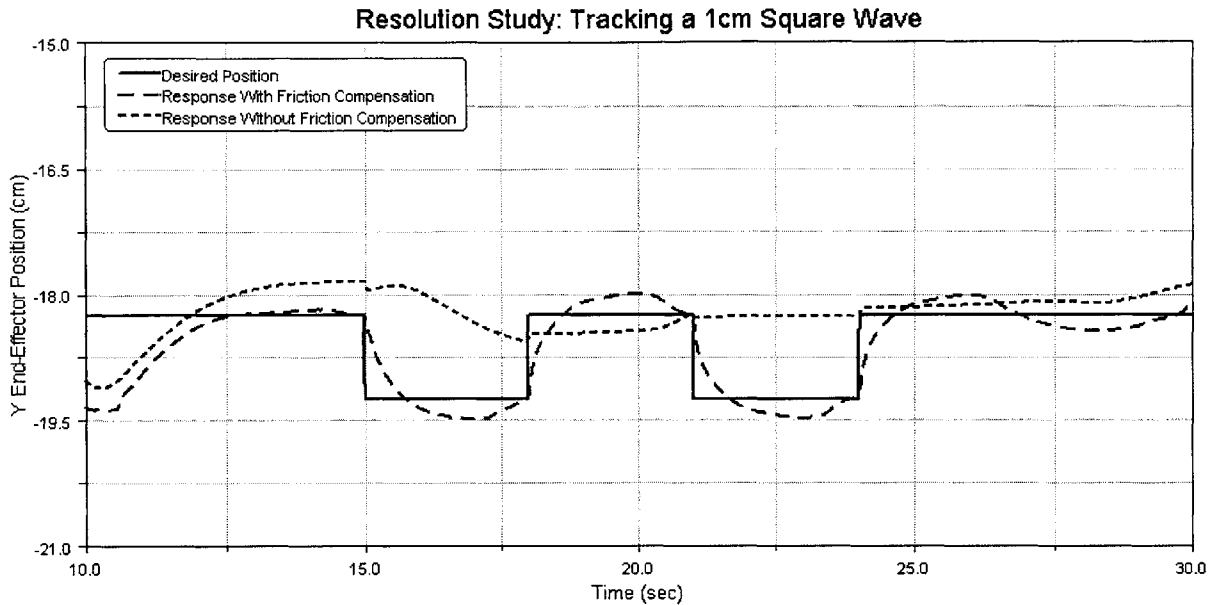


*Figure 4.9. End-effector tracking a 1cm square wave with and without friction compensation*

The results show that the position controller is able to respond to the commanded trajectory with a reasonable amount tracking error ( $< 3\text{mm}$ ). This demonstrates the controller's ability to perform fast corrective motions as little as 1 cm in magnitude. The results also demonstrate again how important effective friction compensation is to the controller's capability. Without friction compensation, the control system is virtually unresponsive to a 1cm Cartesian trajectory at this frequency. The commanded motions would need to be significantly larger and/or slower, reducing the operational efficiency of the manipulator.

### 4.3.4 Repeatability Study

Another important performance measure for the position controller is *repeatability*. Repeatability is a measure of the controller's ability to move to a given position over and over again with consistent results. A repeatable system is one that can reliably deliver the same level of capability over time from different points in its operational space. Repeatability is also important to provide the human operator with a consistent control response that he/she can adapt to and become efficient with.

To test the repeatability of the position control, a special trajectory was prepared for the end-effector. To begin, the end-effector is commanded to a position similar to point **D** in the representative heavy-payload task. From this position, the end-effector is then commanded to follow 25 individual trajectories. Each of the 25 trajectories leads away from the starting point in a random direction and then returns along the same path. The average departure of each random trajectory from the starting point is 8.6 cm and the peak velocity for each trajectory is 5 cm/s. Following each of the 25 random trajectories the controller is given 2 seconds of settling time. Figure 4.10 shows the complete path of the end-effector in base-coordinates.

Using this trajectory, a full simulation was run with a 3000 lb payload attached at the end-effector. For comparison, the first 15 random trajectories were repeated in a second simulation with friction compensation disabled. Figure 4.11 shows the positions of the end-effector after returning from each of the random trajectory segments and settling for 2 seconds. Table 4.5 summarizes the results in regard to the absolute translational error of the end-effector position after each random trajectory.

*Table 4.5. Translational error results for the repeatability study*

	<u>Maximum Error</u>	<u>Mean Error</u>
W/ Friction Compensation:	4.3 mm	2.2 mm
W/O Friction Compensation:	83.7 mm	28.8 mm

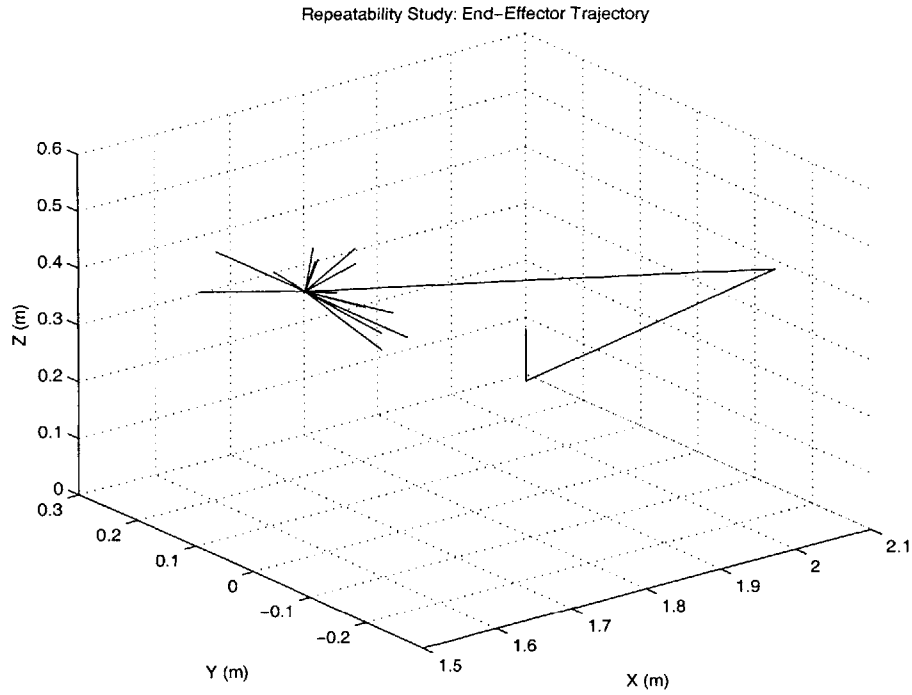


*Figure 4.10. End-effector trajectory, tracking 25 random motions from a set-point*

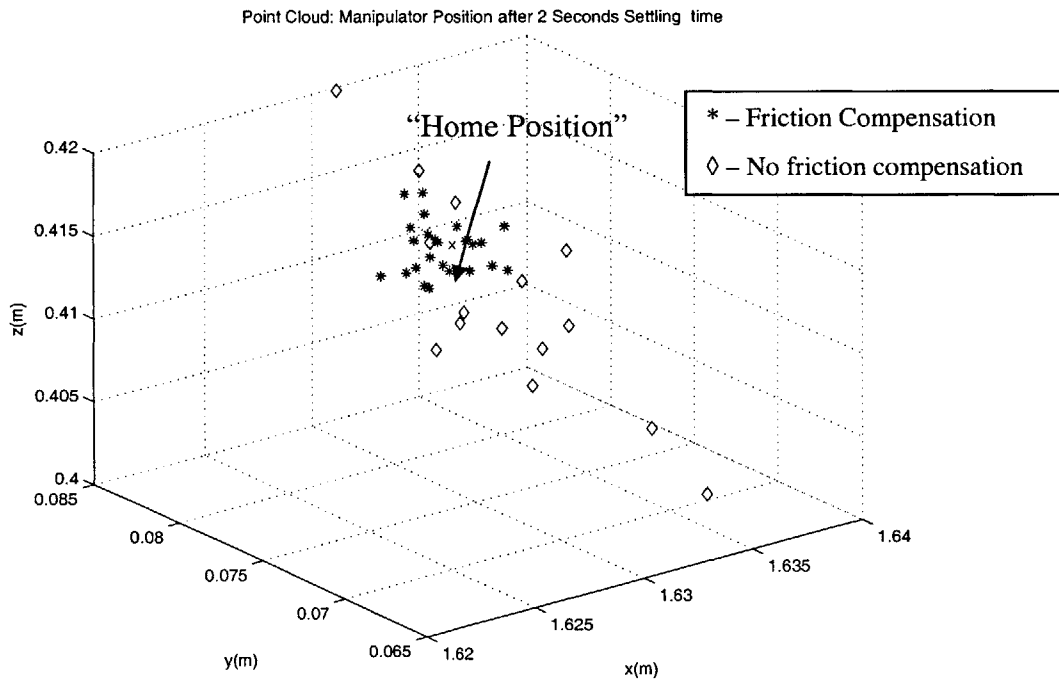


*Figure 4.11. End-effector positions after each random motion and 2 seconds of settling time, with and without friction compensation*

With friction compensation, the mean position error is less than 3 mm. The control system therefore has a very high level of repeatability. Without friction compensation, the mean error increases to 2.9 cm which exceeds the target specification on translational tracking error for the system. Again, effective friction compensation is critical in achieving the target level of performance for this system.

### 4.3.5 Preliminary Analysis of Ship Motion Effects

To test position controller's ability to compensate for ship motions, data was obtained from the manipulator's designer containing the expected worst-case rotations and accelerations experienced by the manipulator due to ship motions. This data consists of estimated magnitudes and periods for each type of ship motion as would be measured by the manipulator's motion sensors during operation. These values are shown in the tables below.

*Table 4.6. Periods and amplitudes for simulated base rotations*

	<u>Amplitude</u>	<u>Period</u>
Pitch:	2°	10.5 seconds
Roll:	13°	20.8 seconds

*Table 4.7. Periods and amplitudes for simulated translational base accelerations*

	<u>Amplitude</u>	<u>Period</u>
Vertical	.354 g	20.8 seconds
Longitudinal	.078 g	20.8 seconds
Transverse	.144 g	20.8 seconds

For this analysis, each type of motion was modeled as a sine wave using the amplitudes and periods listed above. The resulting motions were then added to the ADAMS manipulator model for simulation. The pitch and roll motions were applied to the manipulator's base using the origin of the base coordinates as the center of rotation as shown in Figure 4.12.

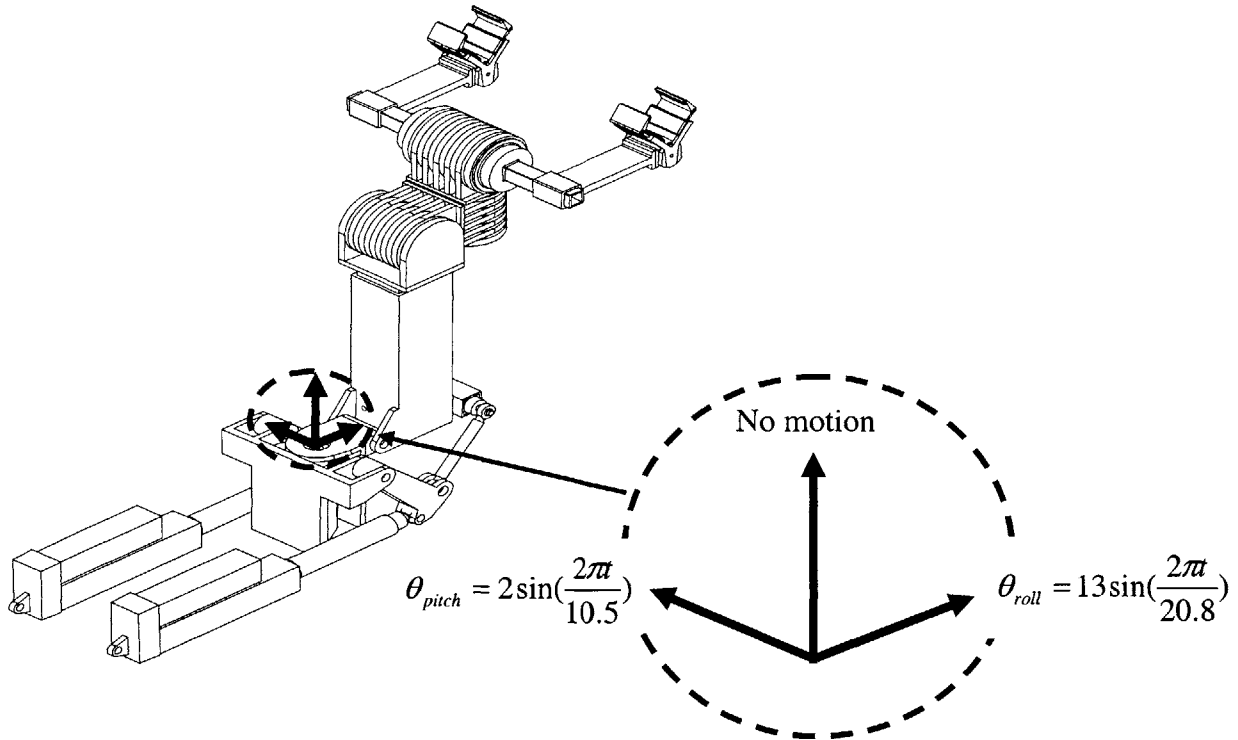


Figure 4.12. Application of base rotations to the simulated manipulator model (adapted from Foster Miller Inc.)

The translational accelerations were applied equally to each of the manipulator's links and the payload by adding them to the model's gravity field as follows:

$$\mathbf{g} = \begin{bmatrix} a_x \\ a_y \\ a_z \end{bmatrix} = \mathbf{R}_x(\theta_{roll})\mathbf{R}_y(\theta_{pitch}) \begin{bmatrix} 0 \\ 0 \\ -9.81 \end{bmatrix} + \begin{bmatrix} 0.078A(t) \\ 0.144A(t) \\ 0.354A(t) \end{bmatrix} \quad (4.1)$$

$$A(t) = 9.81 \sin\left(\frac{2\pi t}{20.8}\right) \quad (4.2)$$

where  $\mathbf{R}_X(\theta_{roll})$  and  $\mathbf{R}_Y(\theta_{pitch})$  are the rotation matrices that transform the inertial gravity vector into the manipulator's base coordinates.

Simulations of the representative light-payload task were performed to study the effects of the ship motions with and without compensation. The resulting Cartesian tracking error for these simulations is shown in Figure 4.13.

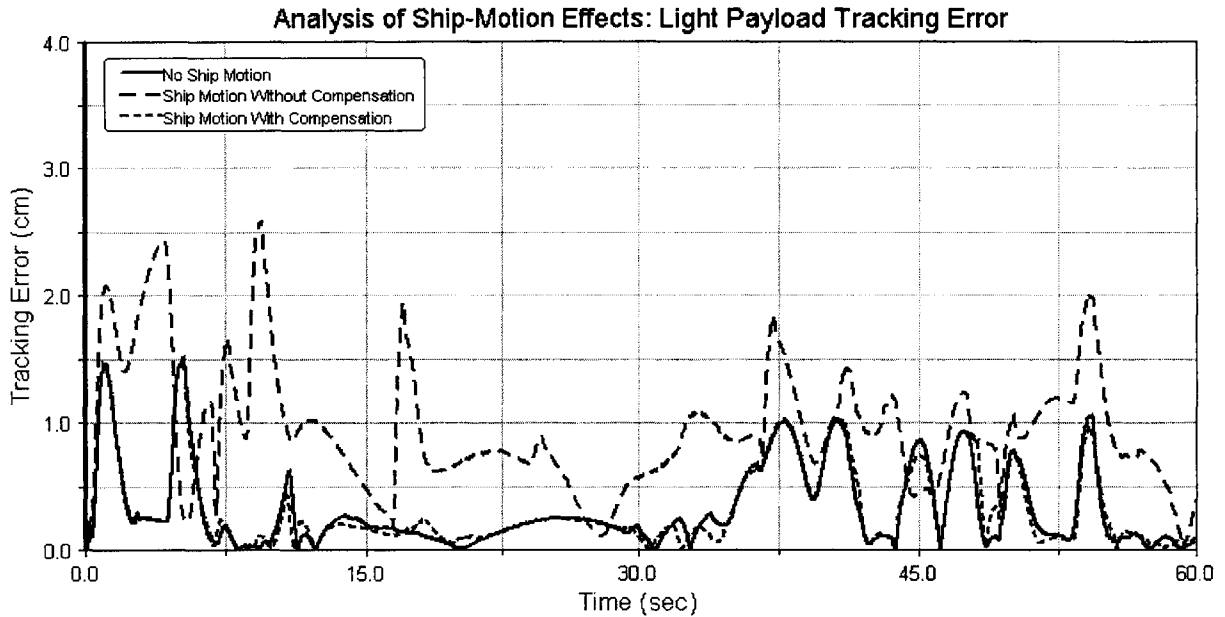


*Figure 4.13. Translational tracking error with simulated base motions*

Without compensation, the peak tracking error is nearly doubled as a result of the ship motions. The controller's compensation, however, is able to eliminate nearly all of the effects of ship motion in the system response. The peak and average tracking errors in the case with compensated ship motion are virtually identical to those in the case with no ship motion at all. The small differences in tracking that remain between these two cases are due to the combined effects of rotational accelerations, centripetal forces, and coriolis forces that are not modeled in the ship motion compensation. One can expect

these uncompensated effects to become larger as the payload mass increases. Future work with this system will include a more in-depth study of these effects.

### 4.3.6 Friction Model Extraction

This section presents an example of the friction model extraction procedure described in Section 3.7. This example consists of extracting a friction model for joint 6 using recorded data from a simulation of the representative light-payload task. The purpose of this exercise is to validate both the feasibility of the model extraction process and the capability of the adaptive estimators to accurately identify the joint friction.

For this example, the extracted friction model is assumed to have the same form as the simulated friction as defined in Section 3.4.2. As a result, it is possible for the extracted model to represent the simulated friction perfectly with no un-modeled effects. For this exercise, therefore, the accuracy of the extracted model is limited only by the accuracy of the adaptive friction estimates. In reality, the joint friction will likely contain behaviors that are not modeled in the assumed form of the extracted friction models. These un-modeled behaviors will further limit the accuracy of the extracted friction models. Studies have been planned beyond this thesis to investigate and quantify the extent of these effects.

Referring to Section 3.4.2, the assumed form of the extracted friction model is as follows:

$$\hat{\tau}_{friction} = -(1 + \sigma_1 |\dot{q}|)(\sigma_2 + \sigma_3 |\tau_{motor}| + \sigma_4 \tau_{motor}^2) \text{sgn}(\dot{q}) \quad (4.3)$$

The goal of the model extraction process is to identify the parameters  $\sigma_1$ ,  $\sigma_2$ ,  $\sigma_3$ , and  $\sigma_4$ . This is accomplished by conducting a curve-fit of the recorded simulation data which consists of the independent variables  $\dot{q}(t)$  and  $\tau_{motor}(t)$ , as well as the friction estimates  $\hat{\tau}_{friction}(t)$ .

Using data recorded from a simulation of the representative light-payload task, a friction model was extracted for joint 6 in the following steps:

1. The true simulated joint friction profile  $\tau_{friction}(\dot{q}(t), \tau_{motor}(t))$  was plotted first to provide a basis of comparison for the extracted model.
2. The friction estimates  $\hat{\tau}_{friction}$  were then plotted as a function of  $\dot{q}(t)$  and  $\tau_{motor}(t)$  using the recorded data.
3. In preparation for the curve-fit procedure, the adaptive friction estimates near zero velocity were removed. The initial “learning curve” transient in the adaptive estimates was also removed.
4. Using the remaining data, a nonlinear least-squares curve fit was computed to identify the parameters  $\sigma_1$ ,  $\sigma_2$ ,  $\sigma_3$ , and  $\sigma_4$ .
5. The parameters  $[\sigma_1, \sigma_2, \sigma_3, \sigma_4]$  were finally inserted into Equation 4.3 to yield the extracted friction model defining  $\hat{\tau}_{friction}(\dot{q}, \tau_{motor})$ . This model was then used to predict the joint friction for all values of  $\dot{q}$  and  $\tau_{motor}$ .

Figures 4.14 - 4.18 illustrate each of the steps in the above procedure.

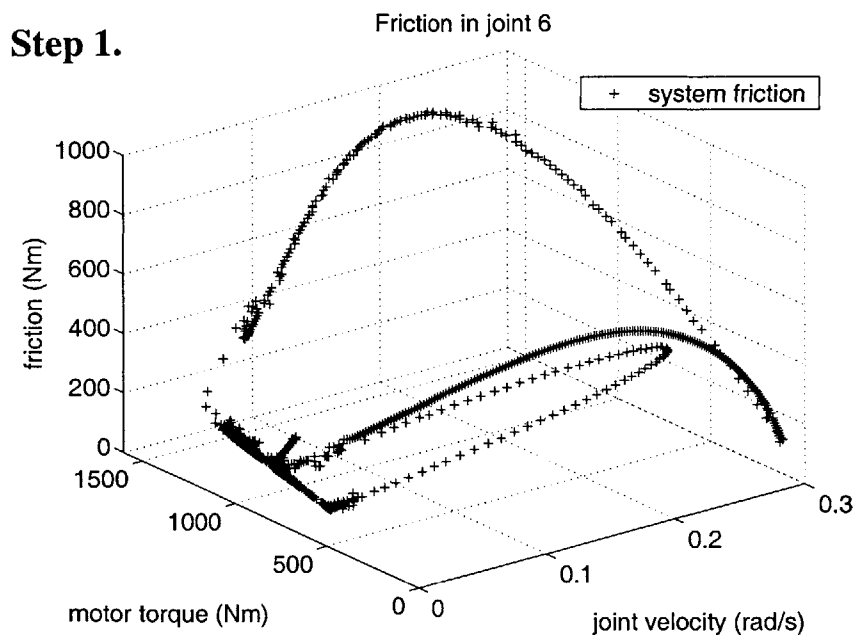


Figure 4.14. Identification of friction parameters using recorded friction estimates: magnitude of simulated friction

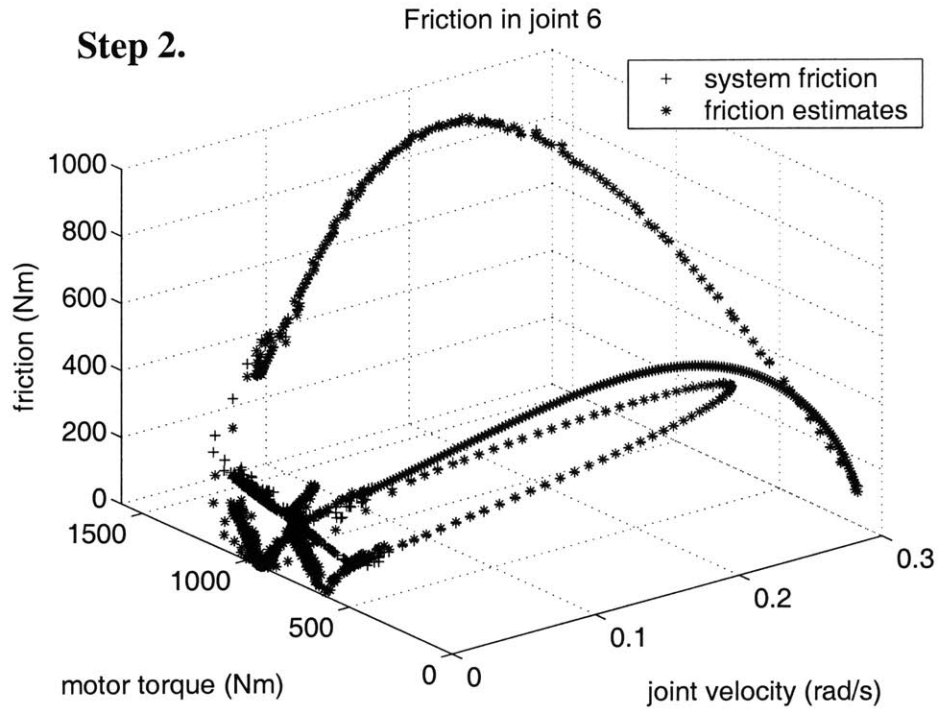


Figure 4.15. Identification of friction parameters using recorded friction estimates: magnitude of simulated friction w/ friction estimates

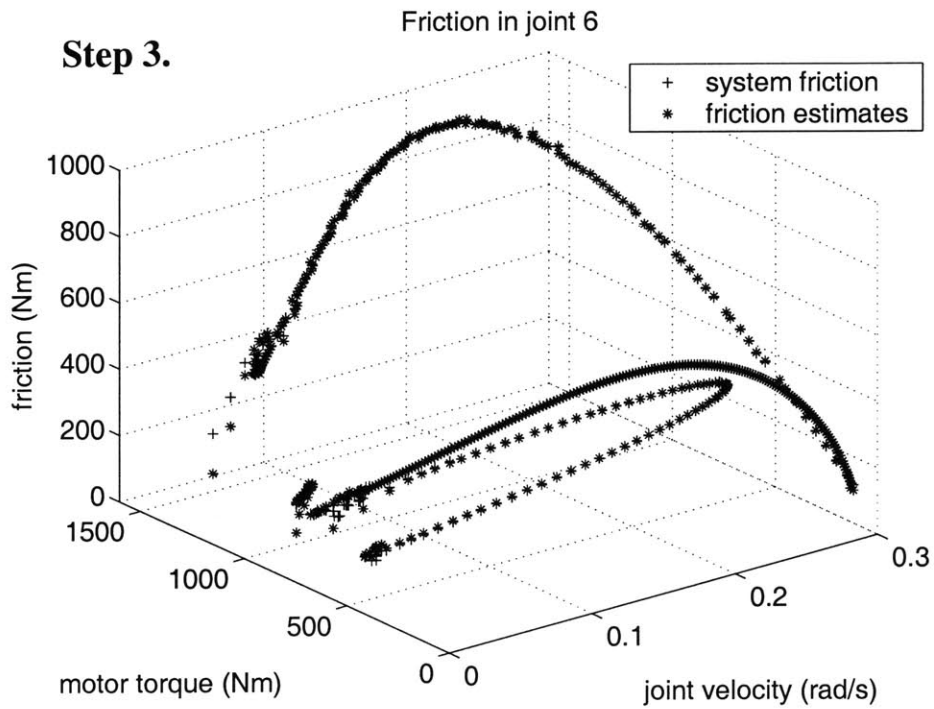


Figure 4.16. Identification of friction parameters using recorded friction estimates: magnitude of simulated friction w/ filtered friction estimates

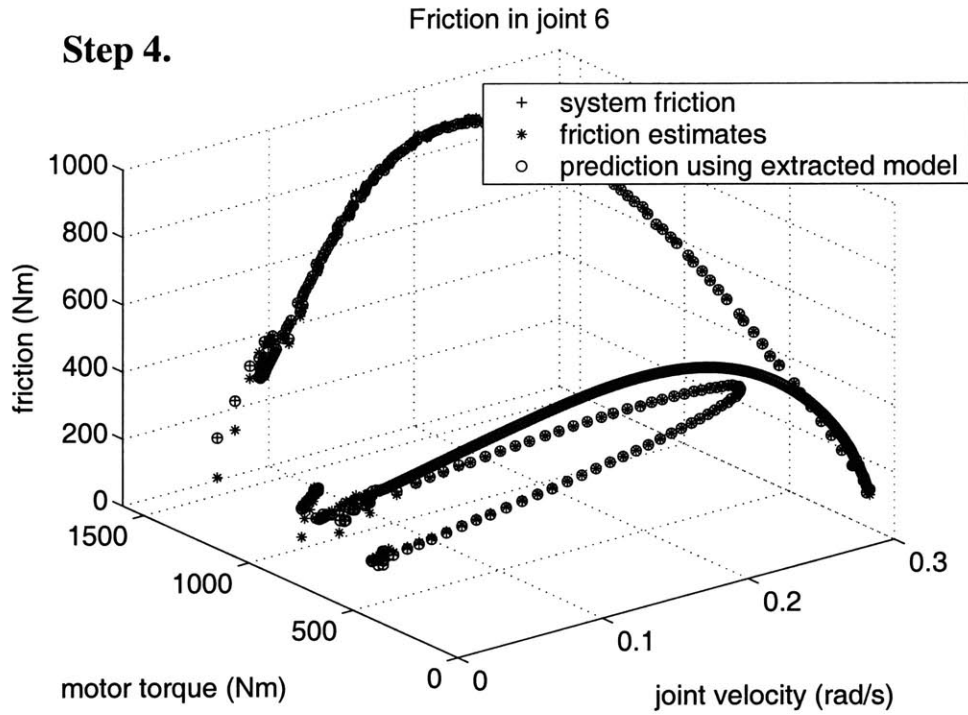


Figure 4.17. Identification of friction parameters using recorded friction estimates: magnitude of simulated friction w/ filtered friction estimates and curve-fit

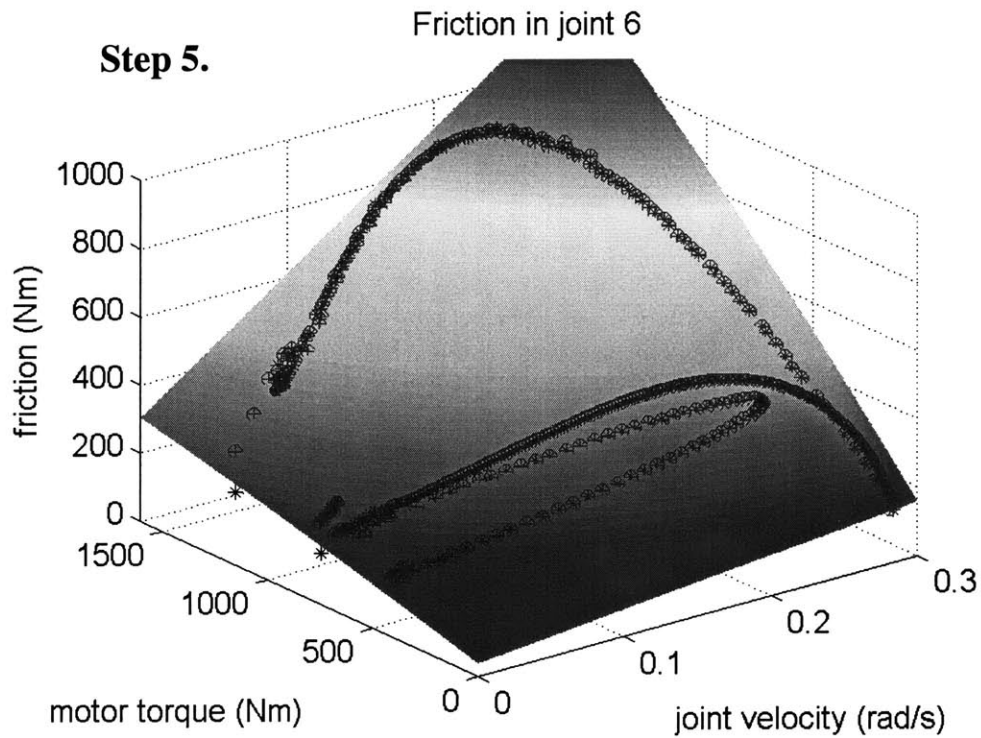


Figure 4.18. Identification of friction parameters using recorded friction estimates: magnitude of simulated friction w/ filtered friction estimates, curve-fit, and predicted friction profile

The accuracy of the extracted friction model  $\hat{\tau}_{friction}(\dot{q}, \tau_{motor})$  is measured by its percent deviation from the actual friction torque as follows:

$$\text{Error}(t) = 100 * \frac{|\hat{\tau}_{friction}(\dot{q}(t), \tau_{motor}(t)) - \tau_{friction}(\dot{q}(t), \tau_{motor}(t))|}{\tau_{friction}(\dot{q}(t), \tau_{motor}(t))} \quad (4.4)$$

The mean and standard deviation of Error(t) for the extracted model above is given in Table 4.8.

*Table 4.8. Error results for the extracted friction model*

	<u>Mean</u>
Error(t):	0.44%

This result indicates that the adaptive estimator for joint 6 was able to identify the joint friction with better than 99% accuracy during this simulation. Because the extracted friction model and the simulated friction model use the same form, the extracted model is able to predict the simulated friction with the same level of accuracy. In practice, however, the real joint friction will not exactly follow the form assumed for the extracted model. There will be un-modeled behaviors in the true friction that will lead to errors in the extracted model despite the accuracy of the adaptive estimates. Future studies will examine the extent of these effects and the impact they have on the control system's overall performance.

## 4.4 Summary and Conclusions

This chapter has presented the results of extensive simulation studies that validate the capability of the control system architecture presented in Chapters 2 and 3. It was shown that the control system is able to perform within the target specifications for both heavy and light-payload tasks, representing the entire operational spectrum for the manipulator. The controller's resolution was shown to be on the order of 1 cm, which

will allow the human operator to make small position adjustments to achieve precise and efficient positioning. It was also shown that the controller has a high level of repeatability and is thus capable of providing consistent performance over a large range of motions. A preliminary analysis of ship-motion effects showed that the control system is able to effectively compensate for these effects without a measurable loss in performance. Finally, it was shown that the controller's adaptive friction estimation is capable of identifying parametric models of the joint friction with better than 99% accuracy in the absence of un-modeled effects.

A prevailing theme in the results presented in this chapter is the control system's effective compensation of joint friction. Without this compensation, it would be impossible for the system to perform within the target specifications. One of the most important challenges for the system, therefore, will be providing the same level of effective compensation when the manipulator is in contact with the environment and adaptive estimation cannot be used. For these intervals, it will be critical to have a good understanding of the joint friction's behavior so that its effects can be completely and accurately modeled in the model extraction process.

## 5.1 Contributions of this Work

This thesis has presented the design of a position control system to allow high-precision, low-bandwidth control of a 6 DOF serial manipulator in a dynamic environment.

Chapter 2 presented a robust design for Cartesian end-effector control using existing methods of decentralized linear control at the joint level coupled with the Jacobian-inverse method of calculating the inverse manipulator kinematics. The linear joint controllers use gain scheduling to provide a stable and consistent response characteristic for the manipulator's large range of payloads. The bandwidth of the joint controllers is limited to guarantee stability without modeling manipulator flexibility in the control system. The control system allows operation in the vicinity of kinematically-singular manipulator positions by temporarily switching from Cartesian tracking to direct-joint control.

Chapter 3 presented a nonlinear disturbance compensation scheme to augment the linear joint-control architecture described in Chapter 2. Disturbance compensation is achieved using a combination of adaptive and sensor-based methods to compensate for the effects of gravity, base motions, and joint friction. To compensate for gravity and base-motion effects, the controller uses a quasi-static model of the manipulator together with feedback from motion sensors to compute feed-forward compensation torques for each joint. Joint friction is compensated through a combination of both sensor-based and adaptive methods. For the first three joints, the control system uses torque control to regulate the joint torque and eliminate the effects of joint friction. This is made possible

by the presence of force sensors in the transmissions of these three joints. For the last three joints, the control system employs the Friedland-Park adaptive estimation method to identify the magnitude of the joint friction and compensate using motor torques. Finally, because the Friedland-Park algorithm cannot be applied in the presence of contact forces, a procedure is proposed by which a temporary parametric model of the joint friction can be extracted from recorded data and used in a feed-forward manner.

Chapter 4 presented the results of extensive simulations that show various measures of the control system's performance capability. These measures include resolution, repeatability, effectiveness in compensating for major disturbances, and tracking performance in two representative payload tasks. Work is continuing in this area as the manipulator's design is completed and test hardware becomes available.

## **5.2 Suggestions for Future Work**

The control system presented in this thesis is being developed in tandem with the mechanical system with the expectation of eventual widespread system deployment. While the design of the core control system is more or less complete, much work still remains to be done in the areas of evaluation and validation.

There is still a great deal that can be learned about the control system's capabilities through modeling and simulation. Studies are currently underway to study the effects of ship motions in more depth using more complex and realistic models of these motions. It will also be important to measure the system's sensitivity to factors like sensor error, model parameter uncertainty, uncompensated disturbances (wind, etc.), and un-modeled behavior in compensated disturbances (friction and ship motions).

The most important future work will be the validation of this design on test hardware. During this stage of work, the control gains and other low-level system parameters will undergo final tuning. The performance of the system's friction compensation will be of particular interest during hardware testing. It will be important to show that the system can extract sufficiently accurate models of the joint friction online using data from the Friedland-Park estimators. The results presented in Chapter 4 indicate that this will be

contingent on the assumed form of the extracted model rather than the performance of the Friedland-Park estimators. A significant piece of work beyond this thesis, therefore, may consist of advancing or reconsidering the friction models defined in Sections 3.4.1 and 3.4.2.

Hardware testing will likely lead to iteration on the control system parameters. Iteration on low-level design elements is to be expected in the development of any system for deployment in the real world. The core control architecture presented in this thesis, however, provides a framework to achieve the necessary capability in the final manipulator system.

## REFERENCES

---

- Agostini M, Parker G, Groom K, Schaub H, Robinett R. "Command Shaping and Closed-Loop Control Interactions for a Ship Crane." Proceedings of the 2002 American Control Conference, Vol. 3, 8-10, pp. 2298-2304, May 2002.
- Amin J, Friedland B, Harnoy A. "Implementation of a Friction Estimation and Compensation Technique." Control Systems Magazine, IEEE, Vol. 17, Issue 4, pp. 71-76, August 1997.
- Armstrong B, Dupont P, Canudas C. "A Survey of Models, Analysis Tools and Compensation Methods for the Control of Machines with Friction." Automatica, Vol. 30, Issue 7, pp. 1083-1138, July 1994.
- Astrom K. "Theory and Applications of Adaptive Control: A Survey." Automatica, Vol. 19, 471, 1983.
- Astrom K, Hagglund T. "PID Controllers: Theory, Design and Tuning." Research Triangle Park, NC: Instrum. Soc. America, 1995.
- Book W. "Modeling, Design and Control of Flexible Manipulator Arms." P.H.D. Thesis, Department of Mechanical Engineering, April 9, 1974.
- Buss S. "Introduction to Inverse Kinematics with Jacobian Transpose, Pseudoinverse and Damped Least Squares methods." Unpublished Survey, April 2004, Draft available at <http://www.math.ucsd.edu/~sbuss/ResearchWeb/ikmethods/>
- Canudas C, Astrom K, Braun K. "Adaptive Friction Compensation in DC-Motor Drives," IEEE Journal of Robotics and Automation, Vol. 3, Issue 6, pp. 681-685, December 1987.
- Canudas C, Lischinsky P. "Adaptive Friction Compensation with Partially Known Dynamic Friction Model." International Journal of Adaptive Control and Signal Processing, Vol. 11, 65-80, 1997.
- Cheah C, Liu C, Liaw H. "Stability of Inverse Jacobian Control for Robot Manipulator." Proceedings of the 2004 IEEE International Conference on Control Applications, Vol. 1, 2-4, pp. 321-326, September 2004.
- Deeter T, Koury G, Rabideau K, Leahy M, Turner T. "The Next Generation Munitions Handler Advanced Technology Demonstrator Program." Proceedings of the 1997 IEEE International Conference on Robotics and Automation, pp. 341-345, 1997.
- Dubowsky S, Tanner A. "A Study of the Dynamics and Control of Mobile Manipulators Subjected to Vehicle Disturbance." Proceedings of the 4<sup>th</sup> International Symposium of Robotics Research, Santa Cruz, CA, August 1987.
- Dupont P. "The Effect of Friction on the Forward Dynamics Problem." International Journal of Robotics Research, Vol. 12, No. 2, April 1993.
- El-Roy A, Friedland B. "Precision Single-Axis Motion Control System with Friction Compensation." Proceeding of the American Control Conference, Vol. 5, 21-23, pp. 3299-3302, June 1995.

Friedland B, Mentzelopoulou S. "On Estimation of Dynamic Friction." Proceeding of the 32<sup>nd</sup> Conference on Decision and Control, Vol. 2, 15-17, pp. 1919-1924, December 1993.

Friedland B, Park Y. "On Adaptive Friction Compensation." IEEE Transactions on Automatic Control, Vol. 37, Issue 10, pp. 1609-1612, October 1992.

Gomes S, Santos da Rosa V. "A New Approach to Compensate Friction in Robotic Actuators." Proceedings. ICRA '03. IEEE International Conference on Robotics and Automation, Vol. 1, 14-19, September 2003.

Henrichfreise H, Witte C. "Experimental Results with Observer-Based Nonlinear Compensation of Friction in a Positioning System." IEEE International Conference on Robotics and Automation, Vol. 1, 16-20, May 1998.

Huang S, Tan K, Lee T. "Adaptive Motion Control using Neural Network Approximations." Automatica, Vol. 38, Issue 2, pp. 227-233, February 2002.

Iagnemma K. "Manipulator Identification and Control Using a Base-Mounted Force/Torque Sensor." Master's Thesis, Department of Mechanical Engineering, MIT, 1997.

Jagannathan S, Lewis F, Liu K. "Modeling, Control and Obstacle Avoidance of a Mobile Robot with an Onboard Manipulator." Proceedings of the 1993 IEEE International Symposium on Intelligent Control, 25-27, pp. 196-201, August 1993.

Khosla, P. "Some Experimental Results on Model-Based Control Schemes," Proceedings of the 1988 IEEE International Conference on Robotics and Automation, Vol. 3, 24-29, pp. 1380-1385, April 1988.

Kim H, Cho Y, Lee K. "Robust Nonlinear Task Space Control for a 6 DOF Parallel Manipulator." Proceedings of the 41<sup>st</sup> IEEE Conference on Decision and Control, Vol. 2, 10-13, December 2002.

Landau, I. "A Survey of Model Reference Adaptive Systems – Theory and Applications," Automatica, Vol. 10, pp. 353-374, July 1974.

Lischinsky P, Canudas C, Morel G. "Friction Compensation of a Schilling Hydraulic Robot," Proceedings of the 1997 IEEE International Conference on Control Applications, 5-7, pp. 294-299, October 1997.

Love L, Jansen J, Pin F. "Compensation of Wave-Induced Motion and Force Phenomena for Ship-Based High Performance Robotic and Human Amplifying Systems." ORNL/TM-2003/233, October 2003.

Love L, Jansen J, Pin F. "On the Modeling of Robots Operating on Ships." Proceedings of the 2004 IEEE International Conference on Robotics and Automation, Vol. 3, pp. 2436-2443, April 26 – May 1, 2004.

Luh J, Fisher W, Paul R. "Joint Torque Control by Direct Feedback for Industrial Robots." IEEE Transactions on Automatic Control, Vol. 28, No. 1, Feb. 1983.

Morel G, Iagnemma K, Dubowsky S. "The Precise Control of Manipulators with High Joint-Friction Using Base Force/Torque Sensing." Automatica: The Journal of the International Federation of Automatic Control, Vol. 36, No. 7, pp. 931-941, 2000

Meggiolaro M, Dubowsky S. "Improving the Positioning Accuracy of Powerful Manipulators with Application in Nuclear Maintenance." Proceedings of the 16th Brazilian Congress in Mechanical Engineering (COBEM), ABCM, Uberlandia, MG, Brazil, Vol. 15, pp. 210-219, November 2001.

Moreno J, Kelly R, Campa R. "Manipulator Velocity Control using Friction Compensation." IEE Proceedings on Control Theory Applications, Vol. 150, No. 2, March 2003.

Niku S. "Introduction to Robotics Analysis, Systems, Applications." Upper Saddle River, NJ: Prentice Hall, pp. 67-71, 2001.

Niemeyer G, Slotine J. "Performance in Adaptive Manipulator Control." Proceedings of the 27<sup>th</sup> IEEE Conference on Decision and Control, Vol. 2, 7-9, pp. 1585-1591, December 1988.

Olsson H, Astrom K, Canudas C, Gafvert M, Lichinsky P. "Friction Models and Friction Compensation." European Journal of Control, Vol. 4, No. 3, 1998.

Paul R. "Robot Manipulators: Mathematics, Programming, and Control." The MIT Press, Cambridge Massachusetts, 1981.

Pfeffer L, Khatib O, Hake J. "Joint Torque Sensory Feedback of a PUMA Manipulator." IEEE Transactions on Robotics and Automation, Vol. 5, No. 4, pp. 418-425, 1989.

Sciavicco L, Siciliano B. "Modeling and Control of Robot Manipulators." Springer. London. 2000.

Shamma J, Athans M. "Analysis of Nonlinear Gain Scheduled Control Systems." IEEE Transactions on Automatic Control, Vol. AC-35, No. 8, pp. 898-907, 1990.

Slotine J, Li W, "On the Adaptive Control of Robot Manipulators," International Journal of Robotics Research, Vol 6, No. 3, 1987.

Tahboub K. "Observer-Based Control for Manipulators with Moving Bases." Proceedings of the 1997 IEEE/RSJ International Conference on Intelligent Robots and Systems, Vol. 3, 7-11, pp. 1279-1284, September 1997.

Toda M, "An  $H_\infty$  Control-Based Approach to Robust Control of Mechanical Systems with Oscillatory Bases." IEEE Transactions on Robotics and Automation, Vol. 20, No. 2, April 2004.

Townsend A. "Linear Control Theory Applied to a Mechanical Manipulator." S.M. Thesis, Department of Mechanical Engineering, M.I.T., January 1972.

Visioli A, Legnani G. "On the Trajectory Tracking Control of Industrial SCARA Robot Manipulators." IEEE Transactions on Industrial Electronics, Vol. 49, No. 1, February 2002.

Whitney, D.E., "Resolved Motion Rate Control of Manipulators and Human Prostheses." IEEE Transactions on Man-Machine Systems, Vol. MMS-10 No. 2 June 1969.

## APPENDIX A: MANIPULATOR PARAMETERS

Using the standard Denavit-Hartenberg convention [Niku, 2001], the kinematics of the manipulator can be completely defined by the information contained in Table A.1

*Table A.1. Denavit-Hartenberg manipulator parameters  
(courtesy of Foster Miller Inc.)*

Link #	Axis Name	$\alpha_i$	$a_i$ (m)	$\theta_i$	$d_i$ (m)	type	Range
1	Base yaw	$\pi/2$	0.1651	0	0	0	See note 1 below
2	Base pitch	$-\pi/2$	0.2951	0	0	0	$-95^\circ$ to $-25^\circ$
3	Arm extension	$\pi/2$	0.0444	0	0	1	0.921 to 1.327 m
4	End pitch	$-\pi/2$	0.3239	0	0	0	$10^\circ$ to $105^\circ$
5	End Yaw	$\pi/2$	0	0	0.3810	0	$-120^\circ$ to $120^\circ$
6	Roll (up to 1500 lb payload)	0	0.5080	0	0	0	$-45^\circ$ to $225^\circ$
6	Roll (1500 to 3000 lb load)	0	0.3810	0	0	0	$-45^\circ$ to $225^\circ$

When all joints angles are zero, the link coordinate systems are defined as follows:

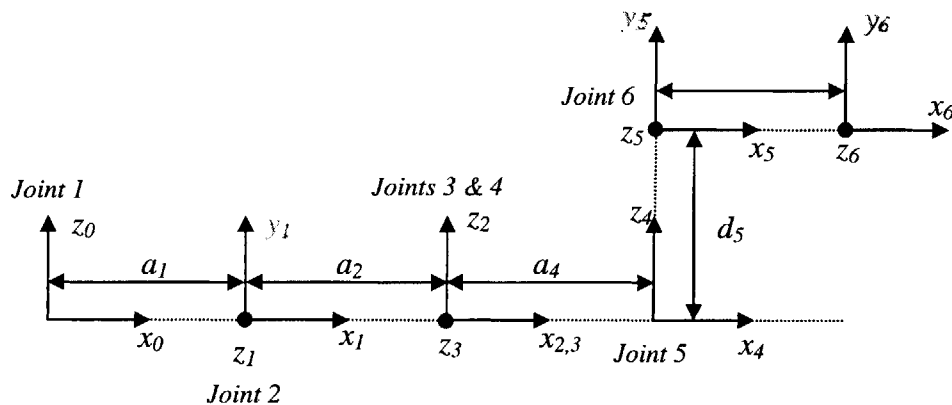


*Figure A.1. Definition of joint coordinate systems with all joint angles at zero (courtesy of Foster Miller Inc.)*

Table A.2 defines the mass, center-of-mass position, and inertia tensor for each link in that link's coordinate system.

*Table A.2. Inertial link parameters  
(courtesy of Foster Miller Inc.)*

Link #	mass(kg)	rx (m.)	ry (m.)	rz (m.)	Ixx (kg m <sup>2</sup> )	Iyy	Izz	Ixy	Iyz	Ixz
1	42.034	-0.092	-.104	0	0.907	0.329	0.995	-0.236	0	0
2	180.184	-.010	0	0.262	17.456	16.76	8.12	-.054	-.033	-.771
3	193.711	-0.023	-0.292	0	21.307	4.814	20.464	-1.036	-.012	-.001
4	137.217	-.198	0	0.011	2.018	4.551	4.595	0	0	-.262
5	140.268	0	-.143	0	5.016	1.73	5.072	0	0	0
6	191.266	-.427	-.018	0	16.2	21.245	6.302	0.883	0	0

Table A.3 defines the mass, center of mass position, and inertia tensor for the representative heavy and light-payloads in the coordinate system of link 6.

*Table A.3. Inertial payload parameters  
(courtesy of Foster Miller Inc.)*

	mass(kg)	rx (m)	ry (m)	rz (m)	Ixx (kg m <sup>2</sup> )	Iyy	Izz	Ixy	Iyz	Ixz
Heavy-payload:	1360.78	-0.127	0.2286	0	927	927	42	0	0	0
Light-payload:	156.0	0	0.2667	0	130	130	0.7	0	0	0

## APPENDIX B: CONTROLLER PARAMETERS

The following are the numerical values of the control gains and other control-related parameters used in simulating the control system. Units are assumed to be in kilograms, meters, seconds, and radians.

### PID Joint Controllers:

PID gains (heavy-payload):

*Table B.1. PID gains for the representative heavy-payload task*

	$K_P$	$K_I$	$K_{D1}$	$K_{D2}$
Joint 1:	210000	200000	40000	110000
Joint 2:	205000	200000	40000	105000
Joint 3:	66500	66000	13000	34000
Joint 4:	33000	33000	6700	17000
Joint 5:	34000	33000	6700	17500
Joint 6:	6800	6700	1300	3500

PID gains (light-payload):

*Table B.2. PID gains for the representative light-payload task*

	$K_P$	$K_I$	$K_{D1}$	$K_{D2}$
Joint 1:	215000	300000	44000	79000
Joint 2:	215000	300000	44000	78000
Joint 3:	73000	100000	15500	27000
Joint 4:	36000	50000	7500	13000
Joint 5:	36000	50000	7500	13000
Joint 6:	7300	10000	1580	2700

Integral saturation limits (all payloads):

*Table B.3. Integral saturation limits*

	$\underline{S}_i$
Joint 1:	3000
Joint 2:	3000
Joint 3:	1000
Joint 4:	500
Joint 5:	500
Joint 6:	100

Torque controllers:

PI control gains (all payloads):

*Table B.4. PI torque-control gains*

	$\underline{K}_P$	$\underline{K}_I$
Joint 1:	2	100
Joint 2:	2	100
Joint 3:	2	100

Adaptive estimators:

Friedland-Park estimator gains (all payloads):

*Table B.5. Friedland-Park estimator gains*

	$\underline{\mu}$	$\underline{k}$
Joint 4:	2	500
Joint 5:	2	300
Joint 6:	2	400

## APPENDIX C: SIMULATED FRICTION PARAMETERS

The following parameter values were used with the models defined in Sections 3.4.1 and 3.4.2 to simulate joint friction in the manipulator. Units are assumed to be in kilograms, meters, seconds, and radians.

### **Static-load-dependent Friction Model (joints 1-3):**

*Table C.1. Parameters for simulated static-load-dependent friction*

	$\alpha_1$	$\alpha_2$	$\alpha_3$	$\beta_1$	$\beta_2$	$\beta_3$
Joint 1:	$37.4 \times 10^{-6}$	0.04	$1 \times 10^{-4}$	0.6	0.4	0.1
Joint 2:	$37.4 \times 10^{-6}$	0.04	$1 \times 10^{-4}$	0.6	0.4	0.1
Joint 3:	$90.0 \times 10^{-6}$	0.04	$1 \times 10^{-4}$	0.6	0.4	0.05

### **Torque-dependent Friction Model (joints 4-6):**

*Table C.2. Parameters for simulated torque-dependent friction*

	$\alpha_1$	$\alpha_2$	$\alpha_3$	$\alpha_4$
Joint 4:	10	500	1.66	$7.8 \times 10^{-5}$
Joint 5:	10	150	1.66	$2.61 \times 10^{-4}$
Joint 6:	10	350	1.66	$1.12 \times 10^{-4}$